03

Calculation of the optical properties of core-mantle spheroids with non-confocal boundaries of the mantle

© V.G. Farafonov[1], V.B. Il'in[1,2,3,¶], S.I. Laznevoi[2], D.G. Turichina[3]

[1] Saint-Petersburg State University of Aerospace Instrumentation,
St. Petersburg, Russia
[2] St. Petersburg State University,
St. Petersburg, Russia
[3] Pulkovo Astronomical Observatory, Russian Academy of Sciences,
St. Petersburg, Russia
¶ e-mail: v.b.ilin@spbu.ru

Received May 14, 2024
Revised June 26, 2024
Accepted June 26, 2024

An exact solution to the problem of light scattering by a spheroidal particle with non-confocal layer boundaries is obtained. The algorithm of the solution presented includes the main achievements of the theory of last years. Using the procedures for calculating spheroidal functions recently created by van Buren, a program has been developed that implements the proposed algorithm in the case of two-layer spheroids. The convergence and accuracy of the solution is investigated for spheroidal particles of 4 types: with the confocal core and envelope, with similar shapes of them, with the most spherical and the most elongated/flattened shape of the core when the core to envelope volume ration is constant. Cross sections of two-layer spheroids of these types calculated at high values of the diffraction parameter (up to $x_a = 2\pi a/\lambda = 120$) are considered and compared with the predictions of the approximate theory of anomalous diffraction. The results of computations of the scattering matrix elements are also presented. They demonstrate that usually considered confocal layer spheroids well describe only the optical properties of particles with similar core and shell shapes.

Keywords: light scattering, T-matrix, layered spheroidal scatterers, optical properties of scatterers.

DOI: 10.61011/EOS.2024.06.59530.6665-24

Introduction

Light scattering by layered spheroidal particles is of great interest for the study of many practical aspects associated with inhomogeneity of individual scatterers as well as of discrete media elements [1–4]. Until recently, focus has been generally made on layered spheroids with confocal layer boundaries, i.e. the boundaries that are the coordinate surfaces in a unified spheroidal coordinate system. Withdrawal of this restriction is a key factor enabling particles with essentially different structures to be addressed — from spheroidal particles with strongly elongated/flattened cores to particles with almost spherical cores.

The issue of light scattering by layered axisymmetric particles, in particular, spheroids, has a sufficiently wide range of comparably simple and often very useful approximate solutions [5,6]. The issue may be resolved more accurately using various numerical methods [7]. These methods have advantages and disadvantages — more uniform approaches are generally more expensive. In particular, numerical methods based on field expansion in basis functions provide relatively more accurate and quick solutions that are generally applicable in a wider parameter domain of a problem, but certainly only for a limited class of scattering particles [8,9]. Selecting a suitable basis is an important factor of such methods.

For arbitrary-shaped particles, a spherical basis is generally used, i.e. fields are written as expansions in spherical wave functions used for spheres in the Mie theory. Then, using the extended boundary condition method (EBCM), the system of integral equations reduces to an infinite system of linear algebraic equations (ISLAE) for unknown scattered field expansion coefficients. The relative simplicity of the used spherical functions has to be compensated by a comparatively narrow domain of applicability of the approach, i.e. the particle shape shall not deviate widely from a spherical one [10]. For example, for layered spheroids, semi-axes ratio of shells following the arbitrary core is limited – $a_i/b_i < \sqrt{2}+1$ [11], though for homogeneous spheroids (and accordingly for the cores of multilayer spheroids), the EBCM method with a spherical basis is applicable at any semi-axes ratio a/b of a particle [12]. These analytically obtained results were supported by the special calculations performed for small particles in the Rayleigh approximation [11,12]. For light scattering, these conclusions are also in full agreement with the numerical calculations [10,14].

A fuller consideration of the problem geometry involves the corresponding spheroidal bases, i.e. spheroidal wave functions shall be used for field expansion. Until recently,

the focus has been generally made on light scattering by confocal layered spheroids [15–18]. The differences in these studies are either in choosing spheroidal wave vector harmonics (scalar potentials) or in choosing a solution method (in fact, in the method of transition between layers). Note that, for layered confocal spheroids, the used EBCM method and separation of variables method (SVM) are equivalent from a theoretical point of view [19], because the problem is solved in a single spheroidal basis, but in view of numerical implementation there are some differences between these methods. The numerical simulation has shown in general that the algorithm proposed in [18] is the most effective for such spheroids. It is equally suitable for particles similar in shape to spheres and for needle-shaped and disc-shaped spheroids, and there is no essential restriction on the number of layers.

For non-confocal spheroids, an adequately considered problem geometry involves using different field expansions in each layer due to the difference of spheroidal systems associated with layer boundaries. Then, boundary conditions shall be satisfied either in differential or in integral form within the SVM or EBCM methods, respectively, with further crosslinking of different expansions of the same fields. Such problem solution was brought to numerical implementation only in [20]. The paper generalized the Mie solution for a multilayer sphere to non-confocal layered spheroids, but using standard spheroidal wave vector harmonics for this. The obtained ISLAE for defining unknown scattered field expansion coefficients is quite bulky, nevertheless some numerical results were obtained for two-layer non-confocal spheroids.

The idea of the new approach to an accurate solution of the problem of light scattering by a layered spheroid with non-confocal layer boundaries when using spheroidal bases was proposed and developed in [21]. However, due to an mistake in the equations, no calculations were provided in [21] and it was even not clear whether such approach works and how well it works. In this work, besides deriving correct equations, the algorithm is changed in view of the recent improvements in such approaches: new normalization of spheroidal functions is used, a complex TE-mode is excluded from consideration, transition to the T-matrix is made, etc. [22]. Results of the first numerical calculations are also provided to understand the convergence and accuracy of the approach, applicability for particles with diffraction parameters almost from the area of geometrical optics, and also some identified features of light scattering by non-confocal two-layer spheroids are shown.

1. Basic relations

1.1. Problem formulation

Consider a two-layer particle whose external (S_1) and internal (S_2) shell boundaries are concentrically coaxial (with a single center line) spheroids with semi-axes a_1, b_1 and a_2, b_2 , respectively (Figure 1). The surfaces S_i may

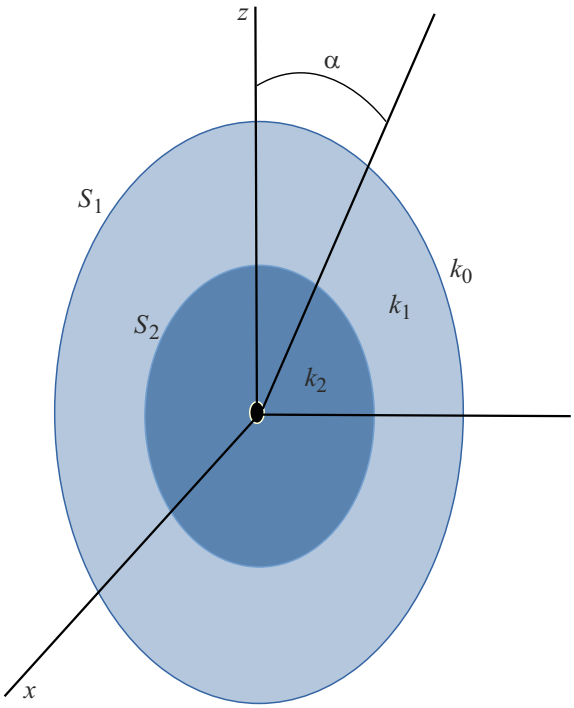

Figure 1. Cross-section of a two-layer spheroidal particle with symbols.

be flattened ($f_i = -1$) and elongated ($f_i = 1$), where the surface number is $i = 1, 2$. An important particular case — confocal shell boundaries when the type of spheroidal surfaces is the same and the inter-focal distances are equal $d_i = 2\sqrt{a_i^2 + b_i^2}$ $(i = 1, 2)$.

Let the plane wave fall on the particle at the angle α to its symmetry axis. Permittivity and magnetic susceptibility of off-particle, particle shell and core media are homogeneous and equal to ε_0, μ_0, ε_1, μ_1 and ε_2, μ_2. The wave number in these media — $k_j = \tilde{k}_0 \tilde{m}_j$, where $\tilde{k}_0 = 2\pi/\lambda$ is the wave number in vacuum, $\tilde{m}_j = \sqrt{\varepsilon_j \mu_j}$ is the refractive index, the layer number $j = 0, 1, 2$.

The coordinate systems are associated with the particle as follows. The Cartesian coordinates (x, y, z) are chosen so that the z axis coincides with the particle center line and the x axis is in the plane that includes the center line and the wave vector $\mathbf{k}$. Spherical coordinates (r, θ, φ) are linked to the Cartesian ones as usual (see relations (1) to (3) below). For the particle surface S_1 and core boundary S_2, the individual spheroidal coordinates (ξ_i, η_i, φ) are introduced, where $i = 1, 2$, therefore

$$x = r \sin\theta \cos\varphi$$
$$= d_i/2\ (\xi_i^2 - f_i)^{1/2}\ (1 - \eta_i^2)^{1/2} \cos\varphi, \qquad (1)$$
$$y = r \sin\theta \sin\varphi$$
$$= d_i/2\ (\xi_i^2 - f_i)^{1/2}\ (1 - \eta_i^2)^{1/2} \sin\varphi, \qquad (2)$$
$$z = r \cos\theta\ =\ d_i/2\ \xi_i\, \eta_i \qquad (3)$$

and S_i is the coordinate surface (with the equation $\xi_i = \xi_{i,0} = \text{const}$ in the system associated with it). In a particular case of two-layer confocal spheroids, a single spheroidal system is sufficient because $d_1 = d_2$.

As usual, we will consider the harmonic fields $\mathbf{E}(\mathbf{r}, \omega)$, $\mathbf{H}(\mathbf{r}, \omega)$, where ω is the frequency, $\mathbf{r}$ is the radius-vector [1]. We will divide all fields into two parts, for example,

$$\mathbf{E}^{(j)} = \mathbf{E}_{\mathrm{A}}^{(j)} + \mathbf{E}_{\mathrm{B}}^{(j)}, \tag{4}$$

where $\mathbf{E}_{\mathrm{A}}^{(j)}$ is regular in the origin of coordinates, and $\mathbf{E}_{\mathrm{B}}^{(j)}$ satisfies the radiation condition at infinity, $j = 0, 1, 2$. Then an unknown scattered field is $\mathbf{E}^{\mathrm{sca}} = \mathbf{E}_{\mathrm{B}}^{(0)}$, and the incident wave is $\mathbf{E}^{\mathrm{in}} = \mathbf{E}_{\mathrm{A}}^{(0)}$. The field in the particle core is apparently regular $\mathbf{E}_{\mathrm{B}}^{(2)} = 0$. As is commonly known, it is sufficient to consider two incident plane wave cases when the electric field vector is perpendicular (transverse electric or TE-mode) and parallel (transverse magnetic or TM-mode) to the plane that includes the wave vector $\mathbf{k}$ and particle center line z [23].

1.2. Solution method

We will mainly follow paper [21] below by noting the most important differences from it. In particular, axisymmetric portion of the fields was additionally identified in [21], which offers some advantages [24]. However, following [25], we won't do this for a more convenient transition to the standard T-matrix.

The scattered field (and, therefore, all optical characteristics of a spheroid) may be found in different ways, including several accurate methods based on field expansion in spheroidal basis. We use EBCM [2]. SVM [2] may serve as another method, but EBCM is more preferable for layered scatterers, because it more conveniently considers boundary conditions than SVM and provides a system of equations to find the scattered field [21].

In EBCM, the Maxwell equations and boundary conditions reduce to the following equations at each media boundary (S_i, $i = 1, 2$) [9]:

$$\nabla \times \int\limits_{S_i} \mathbf{n}_i \times \mathbf{E}^{(i)}(\mathbf{r}')\, G^{(i-1)}(\mathbf{r}, \mathbf{r}')\, ds' - \frac{1}{i\tilde{k}_0 \varepsilon_{i-1}} \nabla \times \nabla \times \int\limits_{S_i} \mathbf{n}_i \times \mathbf{H}^{(i)}(\mathbf{r}')\, G^{(i-1)}(\mathbf{r}, \mathbf{r}')\, ds' = \begin{cases} -\mathbf{E}_{\mathrm{A}}^{(i-1)}(\mathbf{r}), & \mathbf{r} \in D_i, \\ \mathbf{E}_{\mathrm{B}}^{(i-1)}(\mathbf{r}), & \mathbf{r} \in \mathbb{R}^3 \setminus \bar{D}_i, \end{cases} \tag{5}$$

where D_i — is a domain inside S_i, $\bar{D}_i$ is the closure of D_i (includes the domain boundary), $G^{(i)}(\mathbf{r}, \mathbf{r}') = \exp(ik_i|\mathbf{r} - \mathbf{r}'|)/(4\pi|\mathbf{r} - \mathbf{r}'|)$ is Green's function. Equations (5) are obtained using the Stratton–Chu integral identities. For example, when $i = 1$, these identities are written for the incident and scattered light fields $\mathbf{E}_{\mathrm{A}}^{(0)}$ and $\mathbf{E}_{\mathrm{B}}^{(0)}$, therefore Green's function equal to $G^{(0)}$ with the off-particle medium permittivity ..... is used ε_0. By adding these relations and considering the boundary conditions on the particle surface, for example, $\mathbf{n}_0 \times (\mathbf{E}_{\mathrm{A}}^{(0)} + \mathbf{E}_{\mathrm{B}}^{(0)}) = \mathbf{n}_0 \times \mathbf{E}^{(1)}$, the given equations are derived. If $i = 2$, then integral relations for the core shall be addressed in a similar way.

All fields and Green's functions are expanded in series in some basis and, after substitution of the expansions into equations (5) and standard conversions, ISLAE in the scattered (and internal, if required) field expansion coefficients is derived [9]. Solution of the system enables any optical characteristics of the spheroid to be calculated.

We'll use a specific spheroidal basis that is preferable for spheroidal particles [24]. For nonaxisymmetric portions of fields in [21], expansions of the following type (for example, for the TM-mode) were actually used in each particle domain

$$\mathbf{E}(\mathbf{r}) = \sum_{\nu} \left(a_\nu \mathbf{N}_\nu^{\mathbf{z}}(\mathbf{r}) + b_\nu \mathbf{N}_\nu^{\mathbf{r}}(\mathbf{r}) \right). \tag{6}$$

Solutions of the Helmholtz vector equation were used here

$$\mathbf{N}_\nu^{\mathbf{s}}(\mathbf{r}) = \frac{1}{k} \nabla \times \nabla \times (\psi_\nu(\mathbf{r})\, \mathbf{s}), \tag{7}$$

where $\mathbf{s}$ — is the unit coordinate vector $\mathbf{i}_z$ and the radius-vector $\mathbf{r}$ for $\mathbf{N}_\nu^{\mathbf{z}}$ and $\mathbf{N}_\nu^{\mathbf{r}}$, respectively, k is the wave number. Solution of the Helmholtz scalar equation in spheroidal coordinates was chosen as follows [26]

$$\bar{\psi}_\nu^{(q)}(\xi, \eta, \varphi, c) = R_{mn}^{(q)}(c, \xi)\, \bar{S}_{mn}(c, \eta)\, F_{\sigma,m}(\varphi). \tag{8}$$

Here, $\nu = \{\sigma, m, n\}$, where $m = 0, 1, \ldots$, $n = m, m + 1, \ldots$, while $\sigma = e$ and o, when $F_{\sigma,m}(\varphi) = \tilde{c}_m \cos m\varphi$ and $\tilde{c}_m \sin m\varphi$, respectively, $\tilde{c}_m = \sqrt{(2 - \delta_{m,0})/2\pi}$, where $\delta_{m,0}$ is the Kronecker delta symbol. $R_{mn}^{(q)}(c, \xi)$ are the q-th kind ($q = 1, 3$) spheroidal radial functions. c is equal to $kd/2$ and $-ikd/2$ for the elongated and flattened spheroidal coordinates, respectively, d is the inter-focal distance, k is the wave number in the medium. Notation $\bar{\psi}_\nu^{(q)}$ (barred) hereinafter indicates that normalized angular functions $\bar{S}_{mn}(c, \eta) = S_{mn}(c, \eta)/N_{mn}(c)$ are used, where $S_{mn}(c, \eta)$ — are the spheroidal functions, $N_{mn}(c)$ is the normalizing constant. These functions may be defined either according to Flammer $S_{mn}^{\mathrm{F}}(c, \eta)$ [27], or to Meixner–Schäfke $S_{mn}^{\mathrm{MS}}(c, \eta)$ [28], whereby for the normalized functions we have

$$\int\limits_{-1}^{1} |\bar{S}_{mn}^{\mathrm{F}}(c, \eta)|^2\, d\eta = \int\limits_{-1}^{1} |\bar{S}_{mn}^{\mathrm{MS}}(c, \eta)|^2\, d\eta = 1, \tag{9}$$

i.e. $\bar{S}_{mn}^{\mathrm{F}}(c, \eta) = \bar{S}_{mn}^{\mathrm{MS}}(c, \eta)$. Taking into account that the normalizing constants for the first determination are equal to $N_{mn}(c)$, and for the second determination are equal to $-N_{mn}(0)$, directly for the functions themselves we obtain

$$S_{mn}^{\mathrm{F}}(c, \eta)/N_{mn}(c) = S_{mn}^{\mathrm{MS}}(c, \eta)/N_{mn}(0). \tag{10}$$

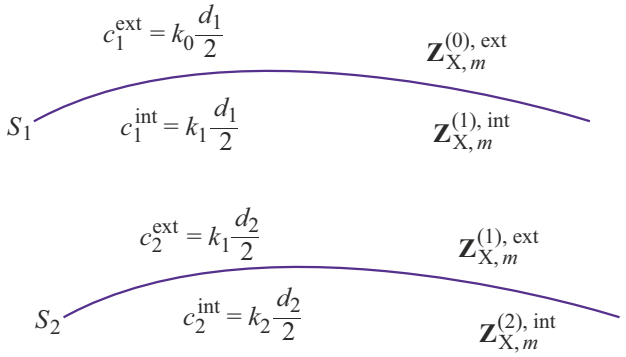

Figure 2. Notations of c and expansion coefficient vectors in various areas of the two-layer particle.

For theoretical and numerical analysis of the spheroidal angular functions, expansion in the associated Legendre functions is generally used:

$$\begin{matrix} S_{mn}^{\text{F}}(c,\eta) \\ S_{mn}^{\text{MS}}(c,\eta) \end{matrix} = \sum_{r=0,1}^{\infty\ \prime} \begin{matrix} d_r^{mn}(c) \\ d_r(c|mn) \end{matrix} P_{m+r}^{m}(\eta). \qquad (11)$$

Taking into account relation (10), from equation (11) we find

$$\bar{d}_r^{mn}(c) = d_r^{mn}(c)/N_{mn}(c) = d_r(c|mn)/N_{mn}(0) = \bar{d}_r(c|mn). \qquad (12)$$

This result is very important for numerical calculations in the given scattering problem. In the problem solution algorithms used before, the occurring integrals of the products of the spheroidal angular functions and their derivatives were represented as series including coefficients $d_r^{mn}(c)$. Equations (12) make it possible to solve the problem using a representation of spheroidal angular functions $S_{mn}^{\text{MS}}(c,\eta)$ that is more favorable on the computational side, when the function values are moderate [29]. Moreover, in contrast with [21], we use normalized angular functions because this provides additional advantages — undesired considerable difference between the expansion coefficients of the spheroidal angular functions in spherical functions is avoided [30].

Field representation (6) is equivalent to the scalar potential expansion U, V, if the fields are introduced properly, i.e.

$$\mathbf{E} = -\frac{1}{i\varepsilon\tilde{k}_0}\nabla\times\nabla\times(U\,\mathbf{i}_z + V\,\mathbf{r}),$$
$$\mathbf{H} = \nabla\times(U\,\mathbf{i}_z + V\,\mathbf{r}). \qquad (13)$$

For expansion of the potential U, V , we assume that each media boundary S_i $(i = 1, 2)$ is associated by it own spheroidal system (ξ_i, η_i, φ), and c included in basis functions (8) depends on the medium parameters. Figure 2 shows notations of c, where ext and int correspond to the external and internal areas of the coordinate surface $S_i (i = 1, 2)$.

Taking into account the introduced notations, expansions of U, V may be written as: for incident radiation

$$\begin{matrix} U_{\text{A}}^{(0)} \\ V_{\text{A}}^{(0)} \end{matrix} = \sum_{m=0}^{\infty}\sum_{n=m}^{\infty} \begin{matrix} a_{\text{A},mn}^{(0),\text{ext}} \\ b_{\text{A},mn}^{(0),\text{ext}} \end{matrix} R_{mn}^{(1)}(c_1^{\text{ext}}, \xi_1)\,\bar{S}_{mn}(c_1^{\text{ext}}, \eta_1)\,F_{\sigma,m}(\varphi); \qquad (14)$$

for scattered radiation

$$\begin{matrix} U_{\text{B}}^{(0)} \\ V_{\text{B}}^{(0)} \end{matrix} = \sum_{m=0}^{\infty}\sum_{n=m}^{\infty} \begin{matrix} a_{\text{B},mn}^{(0),\text{ext}} \\ b_{\text{B},mn}^{(0),\text{ext}} \end{matrix} R_{mn}^{(3)}(c_1^{\text{ext}}, \xi_1)\,\bar{S}_{mn}(c_1^{\text{ext}}, \eta_1)\,F_{\sigma,m}(\varphi); \qquad (15)$$

for radiation within the shell (in the coordinate system associated with S_1)

$$\begin{matrix} U_{\text{A}}^{(1)} \\ V_{\text{A}}^{(1)} \end{matrix} = \sum_{m=0}^{\infty}\sum_{n=m}^{\infty} \begin{matrix} a_{\text{A},mn}^{(1),\text{int}} \\ b_{\text{A},mn}^{(1),\text{int}} \end{matrix} R_{mn}^{(1)}(c_1^{\text{int}}, \xi_1)\,\bar{S}_{mn}(c_1^{\text{int}}, \eta_1)\,F_{\sigma,m}(\varphi), \qquad (16)$$

$$\begin{matrix} U_{\text{B}}^{(1)} \\ V_{\text{B}}^{(1)} \end{matrix} = \sum_{m=0}^{\infty}\sum_{n=m}^{\infty} \begin{matrix} a_{\text{B},mn}^{(1),\text{int}} \\ b_{\text{B},mn}^{(1),\text{int}} \end{matrix} R_{mn}^{(3)}(c_1^{\text{int}}, \xi_1)\,\bar{S}_{mn}(c_1^{\text{int}}, \eta_1)\,F_{\sigma,m}(\varphi); \qquad (17)$$

for radiation within the shell (in the coordinate system associated with S_2)

$$\begin{matrix} U_{\text{A}}^{(1)} \\ V_{\text{A}}^{(1)} \end{matrix} = \sum_{m=0}^{\infty}\sum_{n=m}^{\infty} \begin{matrix} a_{\text{A},mn}^{(1),\text{ext}} \\ b_{\text{A},mn}^{(1),\text{ext}} \end{matrix} R_{mn}^{(1)}(c_2^{\text{ext}}, \xi_2)\,\bar{S}_{mn}(c_2^{\text{ext}}, \eta_2)\,F_{\sigma,m}(\varphi), \qquad (18)$$

$$\begin{matrix} U_{\text{B}}^{(1)} \\ V_{\text{B}}^{(1)} \end{matrix} = \sum_{m=0}^{\infty}\sum_{n=m}^{\infty} \begin{matrix} a_{\text{B},mn}^{(1),\text{ext}} \\ b_{\text{B},mn}^{(1),\text{ext}} \end{matrix} R_{mn}^{(3)}(c_2^{\text{ext}}, \xi_2)\,\bar{S}_{mn}(c_2^{\text{ext}}, \eta_2)\,F_{\sigma,m}(\varphi); \qquad (19)$$

for radiation within the core

$$\begin{matrix} U_{\text{A}}^{(2)} \\ V_{\text{A}}^{(2)} \end{matrix} = \sum_{m=0}^{\infty}\sum_{n=m}^{\infty} \begin{matrix} a_{\text{A},mn}^{(2),\text{int}} \\ b_{\text{A},mn}^{(2),\text{int}} \end{matrix} R_{mn}^{(1)}(c_2^{\text{int}}, \xi_2)\,\bar{S}_{mn}(c_2^{\text{int}}, \eta_2)\,F_{\sigma,m}(\varphi). \qquad (20)$$

For the given plane wave falling at the angle α to the z axis, the expansion coefficients (14) are known. In particular, for the TM-mode they are equal to

$$a_{\text{A},mn}^{(0),\text{ext}} = -\frac{4i^n}{k_0}\sqrt{\frac{\varepsilon_0}{\mu_0}}\frac{\bar{S}_{mn}(c_1^{\text{ext}}, \cos\alpha)}{\sin\alpha}, \qquad b_{\text{A},mn}^{(0),\text{ext}} = 0, \quad (21)$$

where, for example, for the elongated particle $c_1^{\text{ext}} = k_0 d_1/2$. In contrast with [21], we will consider only the TM-mode because, as shown in [31], solution of the problem for a more complex TE-mode easily follows from the solution for the TM-mode.

1.3. Determining the field expansion coefficients

Substitution of the potential expansions and Green's function taking into account (13) into equations (5) for each boundary $(i = 1, 2)$ gives, after standard conversions,

a system of linear equations for each azimuthal number m [21]:

$$\begin{pmatrix} -A^{(i)}_{31,m} & -A^{(i)}_{33,m} \\ A^{(i)}_{11,m} & A^{(i)}_{13,m} \end{pmatrix} \begin{pmatrix} \mathbf{Z}^{(i),\mathrm{int}}_{\mathrm{A},m} \\ \mathbf{Z}^{(i),\mathrm{int}}_{\mathrm{B},m} \end{pmatrix} = \begin{pmatrix} \mathbf{Z}^{(i-1),\mathrm{ext}}_{\mathrm{A},m} \\ \mathbf{Z}^{(i-1),\mathrm{ext}}_{\mathrm{B},m} \end{pmatrix}, \tag{22}$$

where expansion coefficient vectors are introduced and are equal to ($i = 1, 2$; $\mathrm{X} = \mathrm{A}, \mathrm{B}$)

$$\mathbf{Z}^{(i),\mathrm{int}}_{\mathrm{X},m} = \left(\mathbf{x}^{(i),\mathrm{int}}_{\mathrm{X},m}, \mathbf{y}^{(i),\mathrm{int}}_{\mathrm{X},m}\right)^T,$$

$$\mathbf{Z}^{(i-1),\mathrm{ext}}_{\mathrm{X},m} = \left(\mathbf{x}^{(i-1),\mathrm{ext}}_{\mathrm{X},m}, \mathbf{y}^{(i-1),\mathrm{ext}}_{\mathrm{X},m}\right)^T \tag{23}$$

with the following components:

$$x^{(i),\mathrm{int}}_{\mathrm{X},mn} = k_0\, a^{(i),\mathrm{int}}_{\mathrm{X},mn}\, R^{(q)}_{mn}(c^{\mathrm{int}}_i,\ \xi_{i,0}),$$

$$x^{(i-1),\mathrm{ext}}_{\mathrm{X},mn} = k_0\, a^{(i-1),\mathrm{ext}}_{\mathrm{X},mn}\, R^{(q)}_{mn}(c^{\mathrm{ext}}_i,\ \xi_{i,0}), \tag{24}$$

$$y^{(i),\mathrm{int}}_{\mathrm{X},mn} = k_0 \frac{d_i}{2}\, b^{(i),\mathrm{int}}_{\mathrm{X},mn}\, R^{(q)}_{mn}(c^{\mathrm{int}}_i,\ \xi_{i,0}),$$

$$y^{(i-1),\mathrm{ext}}_{\mathrm{X},mn} = k_0 \frac{d_i}{2}\, b^{(i-1),\mathrm{ext}}_{\mathrm{X},mn}\, R^{(q)}_{mn}(c^{\mathrm{ext}}_i,\ \xi_{i,0}). \tag{25}$$

Note that c^{int}_i, c^{ext}_i correspond to Figure 2.

As far as the vectors $\mathbf{Z}^{(j),\mathrm{Y}}_{\mathrm{X},m}$ in equations (22), (23) consist of two parts, then the matrices $A^{(i)}_{ik,m}$ also have a block structure:

$$A^{(i)}_{lk,m} = \begin{pmatrix} \alpha^{(i)}_{lk,m,1} & \beta^{(i)}_{lk,m,1} \\ \alpha^{(i)}_{lk,m,2} & \beta^{(i)}_{lk,m,2} \end{pmatrix}, \tag{26}$$

where the block components $\alpha^{(i)}_{lk,m,s}, \beta^{(i)}_{ik,m,s}$ $(s = 1, 2)$ are the combinations of spheroidal radial functions and integrals of the spheroidal angular functions and their derivatives. In particular, for the TM-mode, the blocks in the first column $A^{(i)}_{31}$ are calculated as follows ($i = 1, 2$):

$$\begin{aligned} \alpha^{(i)}_{31,m,1} =\ & W^{(m)}_{i-1}\, \tilde{\alpha}^{(i)}_{31,m,1} = W^{(m)}_{i-1} \Big\{ R^{(m)}_{3,i-1}\, \Delta^{(m)}_{i-1,i} \\ & - \frac{\varepsilon_{i-1}}{\varepsilon_i} \Delta^{(m)}_{i-1,i}\, \tilde{R}^{(m)}_{1,i} + \left(\frac{\mu_i}{\mu_{i-1}} - 1\right) \xi_{i,0} \\ & \times \left[\xi_{i,0}\, R^{(m)}_{3,i-1}\, Q^{(m)}_{i-1,i} - Q^{(m)}_{i-1,i} \left(I - 2\,\xi^2_{i,0}\, Q^{(m)}_{i,i} \right) \right] \\ & + \left(-\frac{\varepsilon_{i-1}}{\varepsilon_i} - 1 \right) \xi^2_{i,0}\, Q^{(m)}_{i-1,i} \tilde{R}^{(m)}_{1,i} \\ & - \left(\frac{\mu_i}{\mu_{i-1}} - \frac{\varepsilon_{i-1}}{\varepsilon_i} \right) \frac{f_i - \xi_{i,0}}{(\xi^2_{i,0} - f_i)}\, Q^{(m)}_{i-1,i}\, E^{(m)}_{i,i} \Big\}, \end{aligned} \tag{27}$$

$$\begin{aligned} \beta^{(i)}_{31,m,1} =\ & W^{(m)}_{i-1}\, \tilde{\beta}^{(i)}_{31,m,1}\ W^{(m)}_{i-1} \left\{ \left(\frac{\mu_i}{\mu_{i-1}} - 1 \right) f_i\, \xi_{i,0} \right. \\ & \times \left[R^{(m)}_{3,i-1}\, Q^{(m)}_{i-1,i} + 2\,\xi_{i,0}\, Q^{(m)}_{i-1,i}\, Q^{(m)}_{i,i} \right] \Gamma^{(m)}_{i,i} \\ & + \left(\frac{\varepsilon_{i-1}}{\varepsilon_i} - 1 \right) f_i\, \xi_{i,0}\, Q^{(m)}_{i-1,i}\, \Gamma^{(m)}_{i,i}\, \tilde{R}^{(m)}_{1,i} - \left(\frac{\mu_i}{\mu_{i-1}} - \frac{\varepsilon_{i-1}}{\varepsilon_i} \right) \\ & \times \left. \frac{f_i}{\xi^2_{i,0} - f_i} \left[\left(\xi^2_{i,0}\, Q^{(m)}_{i-1,i} - \Delta^{(m)}_{i-1,i} \right) K^{(m)}_{i,i} + \Gamma^{(m)}_{i-1,i} \right] \right\}, \end{aligned} \tag{28}$$

where the matrices R, W and Q are determined below by relations (36) to (40), and the matrix I is a single one. The matrices

$$\begin{aligned} \Delta^{(m)}_{i-1,i} &= \left\{ \delta^{(m)}_{nl}(c^{\mathrm{ext}}_i,\ c^{\mathrm{int}}_i) \right\}^{\infty}_{n,l=m}, \\ \Gamma^{(m)}_{i-1,i} &= \left\{ \gamma^{(m)}_{nl}(c^{\mathrm{ext}}_i,\ c^{\mathrm{int}}_i) \right\}^{\infty}_{n,l=m}, \\ \Gamma^{(m)}_{i,i} &= \left\{ \gamma^{(m)}_{nl}(c^{\mathrm{int}}_i, c^{\mathrm{int}}_i) \right\}^{\infty}_{n,l=m}, \\ K^{(m)}_{i,i} &= \left\{ \kappa^{(m)}_{nl}(c^{\mathrm{int}}_i, c^{\mathrm{int}}_i) \right\}^{\infty}_{n,l=m}, \\ E^{(m)}_{i,i} &= \left\{ \varepsilon^{(m)}_{nl}(c^{\mathrm{int}}_i, c^{\mathrm{int}}_i) \right\}^{\infty}_{n,l=m} \end{aligned} \tag{29, 30}$$

include the following integrals of the normalized spheroidal angular functions and their derivatives for the arguments $c_1 = c^{\mathrm{ext}}_i$ or c^{int}_i and $c_2 = c^{\mathrm{int}}_i$:

$$\delta^{(m)}_{nl}(c_1,\ c_2) = \int_{-1}^{1} \bar{S}_{mn}(c_1,\ \eta_i)\, \bar{S}_{ml}(c_2,\ \eta_i)\, d\eta_i, \tag{31}$$

$$\gamma^{(m)}_{nl}(c_1,\ c_2) = \int_{-1}^{1} \bar{S}_{mn}(c_1,\ \eta_i)\, \bar{S}_{ml}(c_2,\ \eta_i)\, \eta_i\, d\eta_i, \tag{32}$$

$$\kappa^{(m)}_{nl}(c_1,\ c_2) = \int_{-1}^{1} \bar{S}'_{mn}(c_1,\ \eta_i)\, \bar{S}_{ml}(c_2,\ \eta_i)\, (1 - \eta^2_i)\, d\eta_i, \tag{33}$$

$$\varepsilon^{(m)}_{nl}(c_1,\ c_2) = \int_{-1}^{1} \bar{S}'_{mn}(c_1,\ \eta_i)\, \bar{S}_{ml}(c_2,\ \eta_i)\, (1 - \eta^2_i)\, \eta_i\, d\eta_i. \tag{34}$$

Note that $\bar{S}_{mn}(c, \eta)$, $\eta\, \bar{S}'_{mn}(c, \eta)$ are even and odd functions η, when $n - m$ is even and odd, respectively. Therefore for any c_1, c_2, the integrals $\delta^{(m)}_{nl}(c_1, c_2)$ and $\varepsilon^{(m)}_{nl}(c_1, c_2)$ are equal to zero, when $n - l$ is odd, and the integrals $\gamma^{(m)}_{nl}(c_1, c_2)$ and $\kappa^{(m)}_{nl}(c_1, c_2)$ are equal to zero, when $n - l$ is even.

Integrals (31) to (34) are represented as series, for example

$$\begin{aligned} \delta^{(m)}_{nl}(c_1, c_2) = {\sum_{k=0,1}^{\infty}}' & \bar{d}_k(c_1|mn)\, \bar{d}_k(c_2|ml) \\ & \times \frac{2}{2k + 2m + 1} \frac{(k + 2m)!}{k!}, \end{aligned} \tag{35}$$

where the groove at the summation symbol means that summation is only over the even values of k, if $(n-m)$ is even, and vice versa (the same is for $(n-l)$), which due to the above-mentioned parity properties of the spheroidal angular functions.

The spheroidal radial functions are constant in the surface $(\xi_i = \xi_{i,0})$ integrals that initially constitute the matric components $A_{lk}^{(i)}$, and, therefore, these functions are available above only in the following diagonal matrices:

$$R_{q,i-1}^{(m)} = \left\{ \frac{R_{ml}^{(q)\prime}(c_i^{\rm ext},\, \xi_{j,0})}{R_{ml}^{(q)}(c_i^{\rm ext},\, \xi_{j,0})}\, \delta_{nl} \right\}_{n,l=m}^{\infty},$$

$$\tilde{R}_{q,i}^{(m)} = \left\{ \frac{R_{ml}^{(q)\prime}(c_i^{\rm int},\, \xi_{i,0})}{R_{ml}^{(q)}(c_i^{\rm int},\, \xi_{i,0})}\, \delta_{nl} \right\}_{n,l=m}^{\infty}, \tag{36}$$

$$\hat{R}_{q,i}^{(m)}(c,\xi) = \left\{ R_{ml}^{(q)}(c,\xi)\, \delta_{nl} \right\}_{n,l=m}^{\infty}, \tag{37}$$

$$W_{i-1}^{(m)} = -\left[R_{3,i-1}^{(m)} - R_{1,i-1}^{(m)} \right]^{-1} = \left\{ ic_i^{\rm ext}(\xi_{j,0}^2 - f_j) R_{ml}^{(1)}(c_i^{\rm ext},\, \xi_{i,0})\, R_{ml}^{(3)}(c_i^{\rm ext},\, \xi_{i,0})\, \delta_{nl} \right\}, \tag{38}$$

where $R_{ml}^{(q)\prime}(c,\xi)$ – is the derivative of the spheroidal radial function of the q-th kind.

The other matrices in relations (27), (28) are equal to

$$Q_{i-1,i}^{(m)} = Q^{(m)}(c_i^{\rm ext},\, c_i^{\rm int}) = \Delta_{i-1,i}^{(m)}\, Q^{(m)}(c_i^{\rm int},\, c_i^{\rm int}) = \Delta_{i-1,i}^{(m)}\, Q_{i,i}^{(m)}, \tag{39}$$

$$Q_{i,i}^{(m)} = \left[\xi_{i,0}^2 I - f_i \left(\Gamma_{i,i}^{(m)} \right)^2 \right]^{-1}. \tag{40}$$

Thus, two matrix equations are derived:

$$\begin{pmatrix} -A_{31,m}^{(1)} & -A_{33,m}^{(1)} \\ A_{11,m}^{(1)} & A_{13,m}^{(1)} \end{pmatrix} \begin{pmatrix} \mathbf{Z}_{{\rm A},m}^{(1),{\rm int}} \\ \mathbf{Z}_{{\rm B},m}^{(1),{\rm int}} \end{pmatrix} = \begin{pmatrix} \mathbf{Z}_{{\rm A},m}^{(0),{\rm ext}} \\ \mathbf{Z}_{{\rm B},m}^{(0),{\rm ext}} \end{pmatrix} \tag{41}$$

and

$$\begin{pmatrix} -A_{31,m}^{(2)} & -A_{33,m}^{(2)} \\ A_{11,m}^{(2)} & A_{13,m}^{(2)} \end{pmatrix} \begin{pmatrix} \mathbf{Z}_{{\rm A},m}^{(2),{\rm int}} \\ \mathbf{Z}_{{\rm B},m}^{(2),{\rm int}} \end{pmatrix} = \begin{pmatrix} \mathbf{Z}_{{\rm A},m}^{(1),{\rm ext}} \\ \mathbf{Z}_{{\rm B},m}^{(1),{\rm ext}} \end{pmatrix}. \tag{42}$$

It can be seen that an equation is missing that could relate the vectors $(\mathbf{Z}_{{\rm A},m}^{(1),{\rm int}}, \mathbf{Z}_{{\rm B},m}^{(1),{\rm int}})^T$ and $(\mathbf{Z}_{{\rm A},m}^{(1),{\rm ext}}, \mathbf{Z}_{{\rm B},m}^{(1),{\rm ext}})^T$, i.e. the potential expansion coefficients $U^{(1)}$ and $V^{(1)}$ in the shell in the coordinate systems related to S_1 and S_2.

Such relation was found in [32]. In our notations, it is written as $({\rm X} = {\rm A}, {\rm B})$

$$\mathbf{a}_{{\rm X},m}^{(1),{\rm int}} = \Pi_m^{(1)}\, \mathbf{a}_{{\rm X},m}^{(1),{\rm ext}}, \quad \mathbf{b}_{{\rm X},m}^{(1),{\rm int}} = \Pi_m^{(1)}\, \mathbf{b}_{{\rm X},m}^{(1),{\rm ext}}, \tag{43}$$

where the matrix components $\Pi_m^{(1)} = \{\pi_{nl,m}^{(1)}\}$ are written as

$$\pi_{nl,m}^{(1)} = i^{n-l}\, \delta_{nl}^{(m)}(c_1^{\rm int},\, c_1^{\rm ext}) = \sum_{s=m}^{\infty} i^{n-l}\, \bar{d}_{s-m}^{mn}(c_1^{\rm ext})\, \bar{d}_{s-m}^{ml}(c_1^{\rm int})\, N_{ms}^2(0). \tag{44}$$

Hence, taking into account the change of variables (24), (25), we get

$$x_{{\rm X},mn}^{(1),{\rm int}} = \left(\hat{R}_{q,1}(c_1^{\rm int},\, \xi_{1,0})\right) \Pi_m^{(1)} \left(\hat{R}_{q,1}(c_2^{\rm ext},\, \xi_{2,0})\right)^{-1} x_{{\rm X},mn}^{(1),{\rm ext}} = P_{q,m}^{(1)}\, x_{{\rm X},mn}^{(1),{\rm ext}}, \tag{45}$$

$$y_{{\rm X},mn}^{(1),{\rm int}} = \left(\hat{R}_{q,1}(c_1^{\rm int},\, \xi_{1,0})\right) \Pi_m^{(1)} \left(\hat{R}_{q,1}(c_2^{\rm ext},\, \xi_{2,0})\right)^{-1} \frac{d_1}{d_2}\, y_{{\rm X},mn}^{(1),{\rm ext}} = P_{q,m}^{(1)}\, \frac{d_1}{d_2}\, y_{{\rm X},mn}^{(1),{\rm ext}}. \tag{46}$$

So,

$$\mathbf{Z}_{{\rm X},m}^{(1),{\rm int}} = \begin{pmatrix} \mathbf{x}_{{\rm X},m}^{(1),{\rm int}} \\ \mathbf{y}_{{\rm X},m}^{(1),{\rm int}} \end{pmatrix} = \begin{pmatrix} P_{q,m}^{(1)} & 0 \\ 0 & P_{q,m}^{(1)} \frac{d_1}{d_2} \end{pmatrix} \begin{pmatrix} \mathbf{x}_{{\rm X},m}^{(1),{\rm ext}} \\ \mathbf{y}_{{\rm X},m}^{(1),{\rm ext}} \end{pmatrix} = \mathbf{Z}_{{\rm X},m}^{(1),{\rm ext}}. \tag{47}$$

Finally, we get a matrix interconnecting the vectors $\mathbf{Z}_{{\rm X},m}^{(1),{\rm ext}}$ and $\mathbf{Z}_{{\rm X},m}^{(0),{\rm ext}}$ in a relation identical to equation (41),

$$\begin{pmatrix} -\tilde{A}_{31,m}^{(1)} & -\tilde{A}_{33,m}^{(1)} \\ \tilde{A}_{11,m}^{(1)} & \tilde{A}_{13,m}^{(1)} \end{pmatrix}. \tag{48}$$

Blocks of this matrix are defined by

$$\tilde{\alpha}_{ik,m,1}^{(1)} = \alpha_{ik,m,1}^{(1)}\, P_{q,m}^{(1)}, \quad \tilde{\beta}_{ik,m,1}^{(1)} = \beta_{ik,m,1}^{(1)}\, P_{q,m}^{(1)}\, \frac{d_1}{d_2}, \tag{49}$$

$$\tilde{\alpha}_{ik,m,2}^{(1)} = \alpha_{ik,m,2}^{(1)}\, P_{q,m}^{(1)}, \quad \tilde{\beta}_{ik,m,2}^{(1)} = \beta_{ik,m,2}^{(1)}\, P_{q,m}^{(1)}\, \frac{d_1}{d_2}. \tag{50}$$

Combining all derived equations, we have

$$\begin{pmatrix} \mathbf{Z}_{{\rm A},m}^{(0),{\rm ext}} \\ \mathbf{Z}_{{\rm B},m}^{(0),{\rm ext}} \end{pmatrix} = \begin{pmatrix} -\tilde{A}_{31,m}^{(1)} & -\tilde{A}_{33,m}^{(1)} \\ \tilde{A}_{11,m}^{(1)} & \tilde{A}_{13,m}^{(1)} \end{pmatrix} \begin{pmatrix} -A_{31,m}^{(2)} \\ A_{11,m}^{(2)} \end{pmatrix} \mathbf{Z}_{{\rm A},m}^{(2),{\rm int}}, \tag{51}$$

, where the matrix blocks $A_{ik,m}^{(2)}$ shall not be multiplied by $P_{q,m}$, i.e. they are calculated using equations (27), (28).

In [21], the problem solution was correct up to relation (46) and accordingly to the subsequent relations. The error was caused by a wrong change of variables in relations (25) in transitions from $b_{{\rm X},mn}^{(j),{\rm int}}$ to $y_{{\rm X},mn}^{(j),{\rm int}}$ for $j = i$ and $i-1$ (the multiplier $d_i/2$ was omitted). However, the above solution differs from that given in [21] in many important improvements: a) here we used the normalized spheroidal angular functions that offer some advantages during calculations; b) assuming that van Buren

subroutines are used to calculate the spheroidal functions determined according to Meixner and Schäfke, we forwent the determination of these functions according to Flammer as in [21] (for normalized spheroidal functions, the system matrix components are changed); c) clearer notations were introduced in this work (in particular for c_i); d) transition to the T-matrices was made, which is convenient for some mass calculations.

1.4. *T*-matrix and cross-sections

Since the equations underlying the problem solution are linear, the expansion coefficient vectors of the scattered and incident radiation are also related linearly by the so-called T-matrix (transition matrix). In case of spheroids, the T-matrix is known to be broken into unrelated blocks for different azimuthal indices m, i.e.

$$\begin{pmatrix} \mathbf{a}_m^{\mathrm{sca}} \\ \mathbf{b}_m^{\mathrm{sca}} \end{pmatrix} = T_m \begin{pmatrix} \mathbf{a}_m^{\mathrm{in}} \\ \mathbf{0} \end{pmatrix}, \tag{52}$$

where notations .... are introduced for compactness $\mathbf{a}_m^{\mathrm{sca}} = \mathbf{a}_{\mathrm{B},m}^{(0),\mathrm{ext}}$, $\mathbf{b}_m^{\mathrm{sca}} = \mathbf{b}_{\mathrm{B},m}^{(0),\mathrm{ext}}$, $\mathbf{a}_m^{\mathrm{in}} = \mathbf{a}_{\mathrm{A},m}^{(0),\mathrm{ext}}$.

An auxiliary matrix $\tilde{T}_m$ is introduced to relate the expansion coefficient vectors:

$$\begin{pmatrix} \mathbf{x}_{\mathrm{B},m}^{(0),\mathrm{ext}} \\ \mathbf{y}_{\mathrm{B},m}^{(0),\mathrm{ext}} \end{pmatrix} = \begin{pmatrix} \tilde{T}_{11,m} & \tilde{T}_{12,m} \\ \tilde{T}_{21,m} & \tilde{T}_{22,m} \end{pmatrix} \begin{pmatrix} \mathbf{x}_{\mathrm{A},m}^{(0),\mathrm{ext}} \\ \mathbf{y}_{\mathrm{A},m}^{(0),\mathrm{ext}} \end{pmatrix}, \tag{53}$$

where, according to relation (51),

$$\tilde{T}_m = -\left(\tilde{A}_{31,m}^{(1)} A_{31,m}^{(2)} - \tilde{A}_{33,m}^{(1)} A_{11,m}^{(2)}\right)^{-1} \times \left(\tilde{A}_{11,m}^{(1)} A_{31,m}^{(2)} - \tilde{A}_{13,m}^{(1)} A_{11,m}^{(2)}\right). \tag{54}$$

Taking into account that $\mathbf{y}_{\mathrm{A},m}^{(0),\mathrm{ext}} = 0$, we have

$$\mathbf{x}_{\mathrm{B},m}^{(0),\mathrm{ext}} = \tilde{T}_{11,m}\, \mathbf{x}_{\mathrm{A},m}^{(0),\mathrm{ext}}, \quad \mathbf{y}_{\mathrm{B},m}^{(0),\mathrm{ext}} = \tilde{T}_{21,m}\, \mathbf{x}_{\mathrm{A},m}^{(0),\mathrm{ext}}. \tag{55}$$

Finally, for the T-matrix, we obtain

$$T_{11,m} = \left(\hat{R}_{3,m}(c_1^{\mathrm{int}},\, \xi_{1,0})\right)^{-1} \tilde{T}_{11,m} \left(\hat{R}_{1,m}(c_1^{\mathrm{int}},\, \xi_{1,0})\right), \tag{56}$$

$$T_{21,m} = \left(c_1^{\mathrm{int}} \hat{R}_{3,m}(c_1^{\mathrm{int}},\, \xi_{1,0})\right)^{-1} \tilde{T}_{21,m} \left(\hat{R}_{1,m}(c_1^{\mathrm{int}},\, \xi_{1,0})\right). \tag{57}$$

The block matrix $T = \{T_m\}_{m=0}^{\infty}$ derived above for the spheroidal basis is transformed to the standard T-matrix relating the field expansion coefficients in a certain spherical basis according to the relations given in [25]. The last T-matrix is widely used for spheroid assemblies because it enables analytical averaging of cross-sections for them, for example, in random particle orientation.

For an individual particle, the T-matrix is usually irrelevant and is needed to determine the expansion coefficients of an unknown field. Commonly used attenuation and scattering cross-sections are calculated using the following equations

$$C_{\mathrm{ext}} = \frac{4\pi}{k_0^2} \sum_{m=0}^{\infty} \sum_{l=m}^{\infty} i^{-(l-1)} \left(k_0\, a_{ml}^{\mathrm{sca}}\, S_{ml}(\cos\alpha) + i b_{ml}^{\mathrm{sca}} \frac{dS_{ml}(\cos\alpha)}{d\cos\alpha} \right) \sin\alpha, \tag{58}$$

$$C_{\mathrm{sca}} = \frac{\pi}{k_0^2} \sum_{m=0}^{\infty} \sum_{l=m}^{\infty} \sum_{n=m}^{\infty} i^{(n-l)} \left\{ k_0^2\, a_{ml}^{\mathrm{sca}}\, (a_{mn}^{\mathrm{sca}})^*\, \omega_{ln}^{(m)} + i k_0 \left[b_{ml}^{\mathrm{sca}} (a_{mn}^{\mathrm{sca}})^*\, \kappa_{ln}^{(m)} - a_{ml}^{\mathrm{sca}}\, (b_{mn}^{\mathrm{sca}})^*\, \kappa_{nl}^{(m)} \right] + b_{ml}^{\mathrm{sca}} (b_{mn}^{\mathrm{sca}})^*\, \tau_{ln}^{(m)} \right\}, \tag{59}$$

where the asterisk means the complex conjugation, a_{ml}^{sca} and b_{ml}^{sca} are the components of the vectors $\mathbf{a}_m^{\mathrm{sca}}$ and $\mathbf{b}_m^{\mathrm{sca}}$, respectively, α is the angle between the wave vector and spheroid center line. The integral $\kappa_{ln}^{(m)}$ was calculated above and the other integrals are equal to

$$\omega_{nl}^{(m)}(c_1,\, c_2) = \int_{-1}^{1} \bar{S}_{mn}(c_1,\, \eta_i)\, \bar{S}_{ml}(c_2,\, \eta_i)\, (1-\eta_i^2)\, d\eta_i, \tag{60}$$

$$\tau_{nl}^{(m)}(c_1,\, c_2) = \int_{-1}^{1} \left[\bar{S}'_{mn}(c_1,\, \eta_i)\, \bar{S}'_{ml}(c_2,\, \eta_i)\, (1-\eta_i^2) + \frac{m}{(1-\eta_i^2)} \bar{S}_{mn}(c_1,\, \eta_i)\, \bar{S}_{ml}(c_2,\, \eta_i) \right] d\eta_i \tag{61}$$

and are also represented as series [16].

2. Analysis of the numerical calculation results

The approach described in Section 1 was implemented as software written in Fortran 2008. Numerical calculations used the subroutines for calculation of elongated and flattened spheroidal functions developed in [29] and suitable in a wide range of problem parameters, in particular, for the diffraction parameter $x_{\mathrm{a}} = 2\pi a/\lambda \leq 300$, where a is the semi-major axis of the spheroid. For such large particles, the geometrical optics approximation may be often used [25]. For relatively small two-layer spheroids with a confocal core that have $x_{\mathrm{a}} \leq 50$, optical properties were addressed in [16].

2.1. Description of particle structure

The main focus in this work is made on the analysis of numerical calculations of the attenuation, scattering and absorption cross-sections for two-layer particles with different internal structures. To compare the optical properties of such particles, scatterers with identical external surfaces will be considered, i.e. with fixed semi-axes a_1 and b_1. Moreover, fixed ratio of the particle volume to the core volume will be taken, for example, $V_1/V_2 = 2$ (in

other words, the shell and core volumes will be equal). In this case, it is natural to use the same cross-section normalization:

$$\bar{C} = C/\pi r_{\mathrm{V}}^2, \qquad (62)$$

where C_{ext} and C_{sca} are calculated using equations (58), (59), and the absorption cross-section is equal to $C_{\mathrm{abs}} = C_{\mathrm{ext}} - C_{\mathrm{sca}}$. The equivoluminar sphere radius r_{V} depends on the particle shape: $r_{\mathrm{V}} = (a\,b^2)^{1/3}$ and $r_{\mathrm{V}} = (a^2\,b)^{1/3}$ for the elongated and flattened spheroids, respectively.

Four types of two-layer scatterers whose cores are confocal, similar, sphere-shaped and most elongated or flattened. In the latter three cases, focuses of the internal spheroids do not coincide with the focuses of the external spheroidal shell. Note that hereinafter dimensionless linear particle parameters are used for convenience: $x_{\mathrm{a}} = k_0\,a$ and $x_{\mathrm{b}} = k_0\,b$as well as $x_{\mathrm{V}} = k_0\,r_{\mathrm{V}}$.

When considering the two-layer confocal spheroid, the known particle surface coordinate $\xi_{1,0}$ and the core and particle volume ratio $k_{\mathrm{V}} = V_2/V_1$ may be used to find the core surface coordinate by numerical solution of the third-order algebraic equation [16]. For the elongated spheroids in accordance with the Banach theorem, the converging sequence will be obtained using an ordinary iterative method:

$$(\xi_{2,0})_{n+1} = \left[(\xi_{2,0})_n + k_{\mathrm{V}}\left(\xi_{1,0}^3 - \xi_{1,0}\right)\right]^{1/3}, \qquad (63)$$

where $n = 0, 1, 2, \ldots$ and $(\xi_{2,0})_0 = \xi_{1,0}$.

For the flattened spheroids, use the Newton method (i.e. the tangent method):

$$(\xi_{2,0})_{n+1} = \frac{2\,(\xi_{2,0}^3)_n + k_{\mathrm{V}}\left(\xi_{1,0}^3 + \xi_{1,0}\right)}{3\,(\xi_{2,0}^2)_n + 1}, \qquad (64)$$

where $n = 0, 1, 2, \ldots$ and $(\xi_{2,0})_0 = 0$. With the fixed core and volume ratio, the particle surface coordinate may be found using equations (63), (64) after substitution of$\xi_{2,0}$ for$\xi_{1,0}$, of $\xi_{1,0}$ for $\xi_{2,0}$ and of k_{V} for k_{V}^{-1}.

For spheroids with similar layer boundaries, the relation between the core and particle semi-axes may be written as follows: $k_0\,a_2 = k_0\,a_1\sqrt[3]{k_{\mathrm{V}}}$, $k_0\,b_2 = k_0\,b_1\sqrt[3]{k_{\mathrm{V}}}$ both for the elongated and flattened spheroids.

For the flattened particles, the core will have a shape as close to a sphere as possible, if the semi-minor axis of the core is close to the semi-minor axis of the shell, or example, $k_0\,b_2 = 0.99\,k_0\,b_1$. The semi-major axis is determined from the fixed volume condition $k_0\,a_2 = k_{\mathrm{V}}\,k_0\,a_1\,(k_0\,b_1)^2/(k_0\,b_2)^2$. For the flattened particles, we will similarly obtain for a sphere-shaped core$k_0\,b_2 = 0.99\,k_0\,b_1$ and $k_0\,a_2 = k_{\mathrm{V}}[(k_0\,b_1\,(k_0\,a_1)^2/k_0\,b_2]^{1/2}$.

For the fourth type of particles, the most elongated core is calculated using equations $k_0\,a_2 = 0.99\,k_0\,a_1$ and $k_0\,b_2 = k_{\mathrm{V}}[k_0\,a_1(k_0\,b_1)^2/k_0\,a_2]^{1/2}$. For the flattened particles, we will similarly obtain for the most flattened core $k_0\,a_2 = 0.99\,k_0\,a_1$ and $k_0\,b_2 = k_{\mathrm{V}}\,k_0\,b_1(k_0\,a_1)^2/(k_0\,a_2)^2$.

Table 1 and 2 show the parameters of the examined elongated and flattened particles having the same maximum linear diffraction parameter $x_{a_1} = k_0\,a_1 = 40$, as well as the same external surface semi-axes ratio $a_1/b_1 = 2$.

Note that the central cross-sections of these elongated and flattened scatterers coincide. The difference is in that, to obtain the whole particle, the cross-sections shall be rotated about the major axis in the first case and about the minor axis of the external ellipse in the second case.

2.2. Validation of numerical calculations

Within the chosen solution method, electromagnetic fields are represented as infinite series in the chosen spheroidal bases that to the most extent correspond to the problem geometry (in contrast with the spherical basis). Due to this, the validity of obtained numerical results depends on the number of considered terms in these series. As shown before [16], this is the largest particle size together with refractive index (in this case for the non-absorbing particle shell and core it is equal to $m_1 = 1.3$ and $m_2 = 1.5$, respectively) that defines the sufficient number of considered terms $N_{\max}$ over the index n for high-accuracy cross-section calculation. This result has been obtained for relatively small particles with $x_{\mathrm{V}_1} \le 50$. Quite large particles are addressed here, and the above-mentioned statement remains valid considering $N_{\max} = m_2\,x_{\mathrm{a}_1} + 4$. For the above eight particles (Table 1, 2) that have the internal structure with significantly different shape, the number of considered terms shall be equal to $N_{\max} = 64$. The number of terms $M_{\max}$ over m is usually about $N_{\max}/2$ and is defined by the consideration of the convergence of results with increasing number of terms over m [33].

Figure 3 shows a relative computational error of normalized cross-sections $\delta_N = |\bar{C}(N_{\max}) - \bar{C}(N)|/\bar{C}(N_{\max})$ for the above-mentioned types of particles depending on the number of N ($N_{\max} = 96$was chosen for reliability of results). In this case, the relative computational error of cross-sections varies from $10^{-9} - 10^{-10}$ for the flattened and elongated spheroidal particles with confocal or similar core to $10^{-6} - 10^{-8}$ for particles with sphere-shaped or very elongated (flattened) core. The curves in figures break off in case when the next point corresponds to computer zero. Note that the convergence rate is relatively weakly dependent on the core shape (elongated or flattened, confocal or similar), if it differs in shape from the shell not too much. The worst convergence is observed in extreme cases (sphere-shaped, maximum elongated or maximum flattened), when the core surface approaches very closely to the shell surface. This effect is the most vivid for a very flattened core because it is „two-dimensional" in nature in contrast with the elongated particles for which the proximity is observed in one direction.

Table 3 shows the normalized cross-sections for four types of considered elongated particles (for the flattened particles, the situation is similar). Pursuant to the law of conservation of energy, equality of $\bar{C}_{\mathrm{ext}}$ and $\bar{C}_{\mathrm{sca}}$is true for

Table 1. Parameters of the spheroidal cores of the two-layer elongated spheroidal particles with the fixed external surface ($a_1/b_1 = 2, x_{a_1} = k_0 a_1 = 40, x_{V_1} = 2^{1/3} k_0 b_1 = 25.1984$) and fixed core volume

Core shape	$x_{a_2} = k_0 a_2$	$x_{b_2} = k_0 b_2$	a_2/b_2	$x_{r_2} = k_0 r_{V2}$	$x_{d_2} = k_0 d_2/2$
Most elongated	39.6	14.2134	2.7861	20	36.9613
Confocal	37.5890	14.5920	2.5760	20	34.6410
Similar	31.7480	15.8740	2	20	27.4946
Sphere-shaped	20.4061	19.8	1.0306	20	4.9365

Table 2. The same as in Table 1, but for the flattened spheroids at $x_{V_1} = a_1/2^{1/3} = 31.7480$

Core shape	$x_{a_2} = k_0 a_2$	$x_{b_2} = k_0 b_2$	a_2/b_2	$x_{r_2} = k_0 r_{V_2}$	$x_{d_2} = k_0 d_2/2$
Most flattened	39.6	10.2030	3.8812	25.1984	38.2630
Confocal	36.6373	11.9200	3.0734	25.1984	34.6440
Similar	31.7480	15.8740	2	25.1984	27.4946
Sphere-shaped	28.4267	19.8	1.4357	25.1984	20.3970

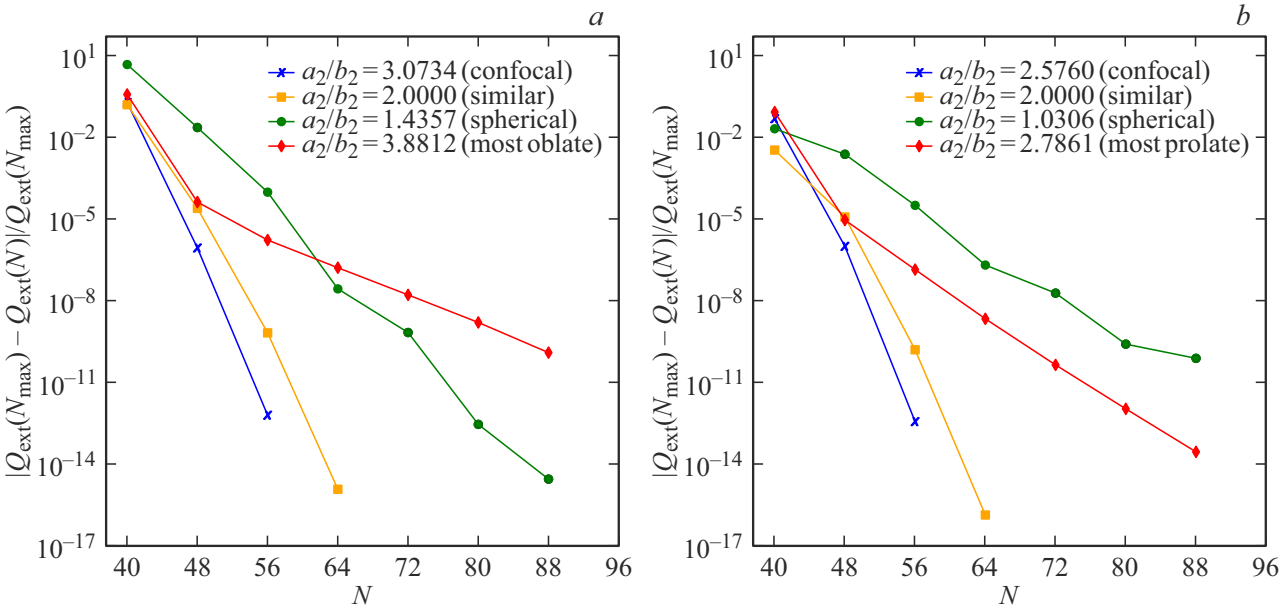

Figure 3. Convergence of the dimensionless attenuation cross-section for different types of two-layer flattened (a) and elongated (b) spheroidal particles (Tables 1, 2) with growth of the number of considered field expansion terms N. Radiation falls parallel to the particle center line ($\alpha = 0$), the refractive indices of the particle shell and core are $m_1 = 1.3$ and $m_2 = 1.5$, respectively, $x_{a_1} = 40$.

non-absorbing particles with the absorption cross-section $\bar{C}_{abs} = \bar{C}_{ext} - \bar{C}_{sca} = 0$, which traditionally serves as the estimation of the absolute computational error of cross-sections. Note that the maximum number of terms in Table 3 was increased to $N_{max} = 96$ in order to decrease the error to 10^{-9} for any particles. When analyzing, it is easy to see that, though the convergence rate of cross-section calculations decreases considerably for particles with extreme cores, the relative error becomes rather high, about 10^{-9}, when the number of considered terms increases up to $N_{max} = 96$. At the same time, to achieve very high accuracy of about 10^{-10} for particles with confocal or similar cores, the one-half lower number of terms is sufficient, as proposed before: $N_{max} = 64$.

When the plane electromagnetic wave falls along the two-layer particle center line ($\alpha = 0$), orientation of the electric field strength vector does not affect the cross-sections, i.e. their values or the TM- and TE-type waves shall coincide

Table 3. Normalized attenuation (ext), scattering (sca) and absorption (abs) cross-sections for two-layer elongated spheroidal particles for the TM- and TE-modes with the different number of considered field expansion terms N ($a_1/b_1 = 2, \alpha = 0, x_{V_1} = 25.198421, x_{V_2} = 20, m_1 = 1.3, m_2 = 1.5$)

N	$\bar{C}^{\mathrm{TM}}$			$\bar{C}^{\mathrm{TE}}$		
	ext	sca	abs	ext	sca	abs
$a_2/b_2 = 2.7861$						
40	1.71E+00	5.13E+01	-4.96E+01	7.66E+00	1.21E+04	-1.21E+04
60	1.87E+00	1.87E+00	-4.24E-08	1.87E+00	1.87E+00	6.03E-08
80	1.87E+00	1.87E+00	-8.62E-11	1.87E+00	1.87E+00	-8.62E-11
96	1.87E+00	1.87E+00	-8.36E-11	1.87E+00	1.87E+00	-8.36E-11
$a_2/b_2 = 2.5760$						
40	1.83E+00	2.61E+00	-7.77E-01	1.28E+00	7.36E+01	-7.23E+01
60	1.93E+00	1.93E+00	-8.62E-11	1.93E+00	1.93E+00	6.51E-08
80	1.93E+00	1.93E+00	-8.62E-11	1.93E+00	1.93E+00	-8.62E-11
96	1.93E+00	1.93E+00	-8.62E-11	1.93E+00	1.93E+00	-8.62E-11
$a_2/b_2 = 2$						
40	1.62E+00	1.70E+00	-7.46E-02	7.76E+00	5.07E+02	-5.00E+02
60	1.63E+00	1.63E+00	-7.34E-11	1.63E+00	1.63E+00	1.76E-08
80	1.63E+00	1.63E+00	-7.30E-11	1.63E+00	1.63E+00	-7.30E-11
96	1.63E+00	1.63E+00	-7.30E-11	1.63E+00	1.63E+00	-7.30E-11
$a_2/b_2 = 1.0306$						
40	1.41E+00	9.43E+00	-8.02E+00	-1.31E+00	2.27E+03	-2.27E+03
60	1.44E+00	1.44E+00	-7.73E-06	1.44E+00	1.44E+00	-7.72E-06
80	1.44E+00	1.44E+00	-4.59E-11	1.44E+00	1.44E+00	-4.59E-11
96	1.44E+00	1.44E+00	-1.36E-10	1.44E+00	1.44E+00	-1.36E-10

completely: $\bar{C}^{\mathrm{TM}} = \bar{C}^{\mathrm{TE}}$. As far as the proposed equations for calculation of the optical properties of particles differ considerably from each other for these two types of incident radiation polarization, then this equality is a very good check for numerical calculations. In the considered cases, the check gives the required results with high accuracy as specified above.

With oblique radiation incidence of the plane wave, the scattering problem is solved independently for each azimuthal index m due to the commutativity of the rotation operator and the operator corresponding to this problem. Then the results shall be summarized over m with the corresponding series being infinite, but the numerical calculations consider a sufficient though finite number of $M_{\max}$ (similar to $N_{\max}$ for n). In [16], convergence of the corresponding numerical results was reviewed and it was found that the sufficient number of terms increases as the particle volume and the refractive index of both the shell and core grow. With the same dimensions and semi-axes ratio, the number of $M_{\max}$ for the elongated particles is multiple time lower than for the flattened ones, and the multiplier is close to a/b. Our calculations for much larger particles have proved these conclusions.

2.3. Calculation of attenuation and scattering factors

To analyze the effects of radiation attenuation, scattering and absorption by the two-layer spheroidal particles depending on their size up to geometric-optical limits, it is natural to use the efficiency factors

$$Q_{\mathrm{x}} = C_{\mathrm{x}}/G, \tag{65}$$

where G is the geometric cross-section of the external spheroid, and x = ext, sca or abs. When the plane wave falls at the angle α to the particle center line $G(\alpha) = \pi b_1 (a_1^2 \sin^2\alpha + b_1^2 \cos^2\alpha)^{1/2}$ and

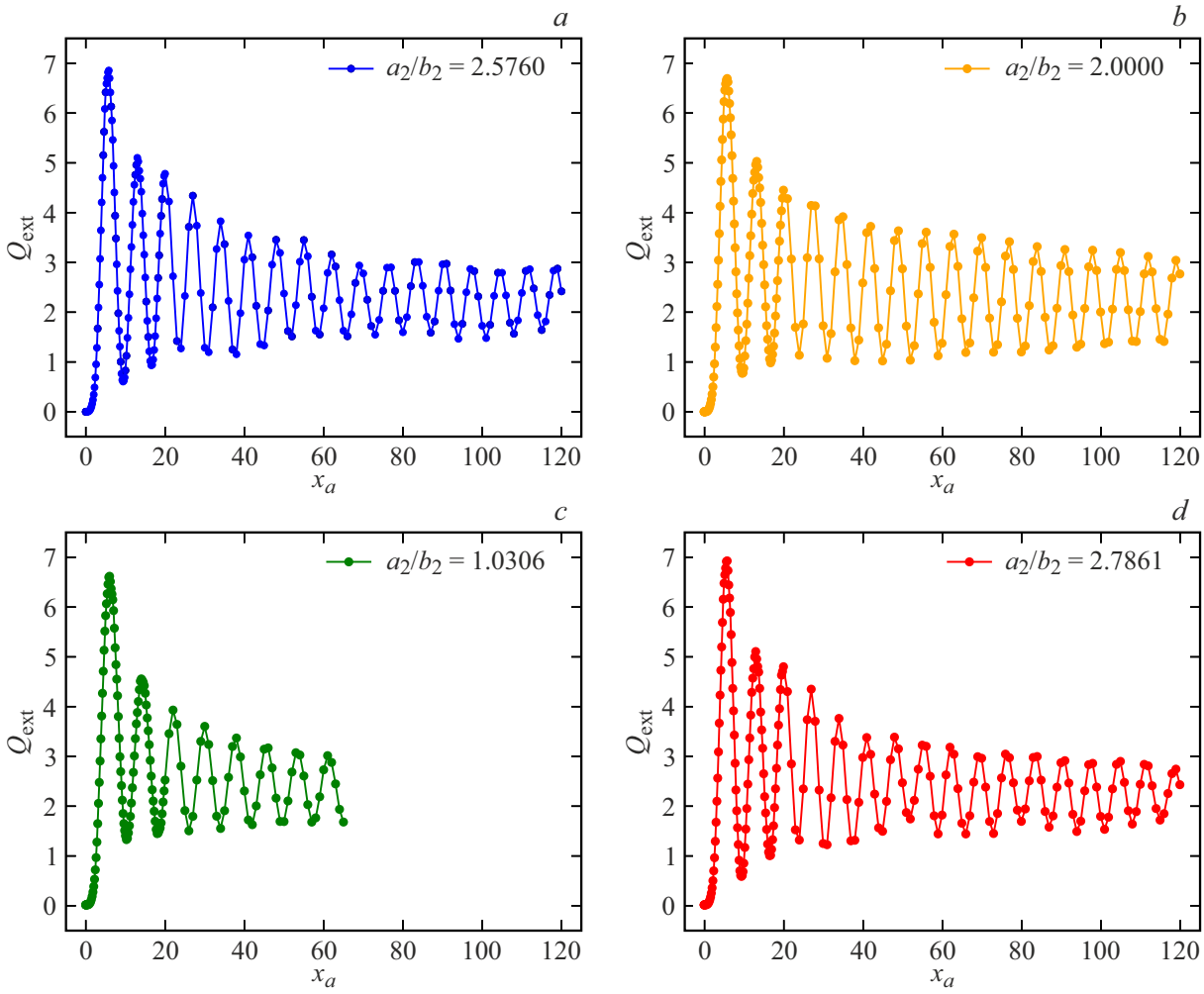

Figure 4. The attenuation efficiency factors Q_{ext} for various types of two-layer elongated spheroidal particles (Table 1) depending on the linear diffraction parameter x_{a_1} with the parallel radiation incidence ($\alpha = 0$) and refractive indices of the shell $m_1 = 1.3$ and core $m_2 = 1.5$.

$G(\alpha) = \pi a_1 (a_1^2 \cos^2\alpha + b_1^2 \sin^2\alpha)^{1/2}$ for the elongated and flattened spheroids, respectively. Note that for the parallel incidence in the first case $G(0) = \pi b_1^2$, and in the second case $G(0) = \pi a_1^2$, while for the perpendicular incidence $G(90) = \pi b_1 a_1$ in both cases.

Relation between the normalized cross-sections and efficiency factors is defined only by the geometrical parameters of the external shell and the angle of incidence of the plane wave α:

$$\bar{C} = \frac{C}{\pi r_v^2} = \frac{(\xi_1^2 - f\cos^2\alpha)^{1/2}}{[\xi_1^4(\xi_1^2 - f)]^{1/6}} Q, \qquad (66)$$

where $f = 1$ and $f = -1$ for the elongated and flattened spheroids, respectively. It follows that the conversion factor for the parallel incidence and perpendicular incidence is equal to $(a_1/b_1)^{-2f/3}$ and $(a_1/b_1)^{f/3}$, respectively. It follows from the above considerations that, for the given particles with a fixed shell, the normalized cross-sections and effective factors have the same dependence on x.

Figures 4 to 7 show that the general behavior of the dependence of Q on the linear diffraction parameter is equivalent to that for homogeneous particles. Alternation of large-scale peaks and valleys results from the interference between the incident and directly transmitted radiation. In the first approximation, this phenomenon, including the extreme values may be described using abnormal diffraction [1]. Peak positions are defined by the phase shift of the central beam

$$\Phi = 2(l_1 - l_2)|m_1 - 1| + 2l_2|m_2 - 1|, \qquad (67)$$

where $2(l_1 - l_2)$ and $2l_2$ are the beam paths (measured in the dimensionless quantities x) in the shell and core, respectively. The oscillation period may be evaluated from $\Delta\Psi = 2\pi$.

In case of the parallel radiation incidence for the two-layer particles with the most elongated core, the central beam propagates almost only in the core, therefore the equation for the oscillation period is written as $2T|m_2 - 1| \approx 2\pi$,

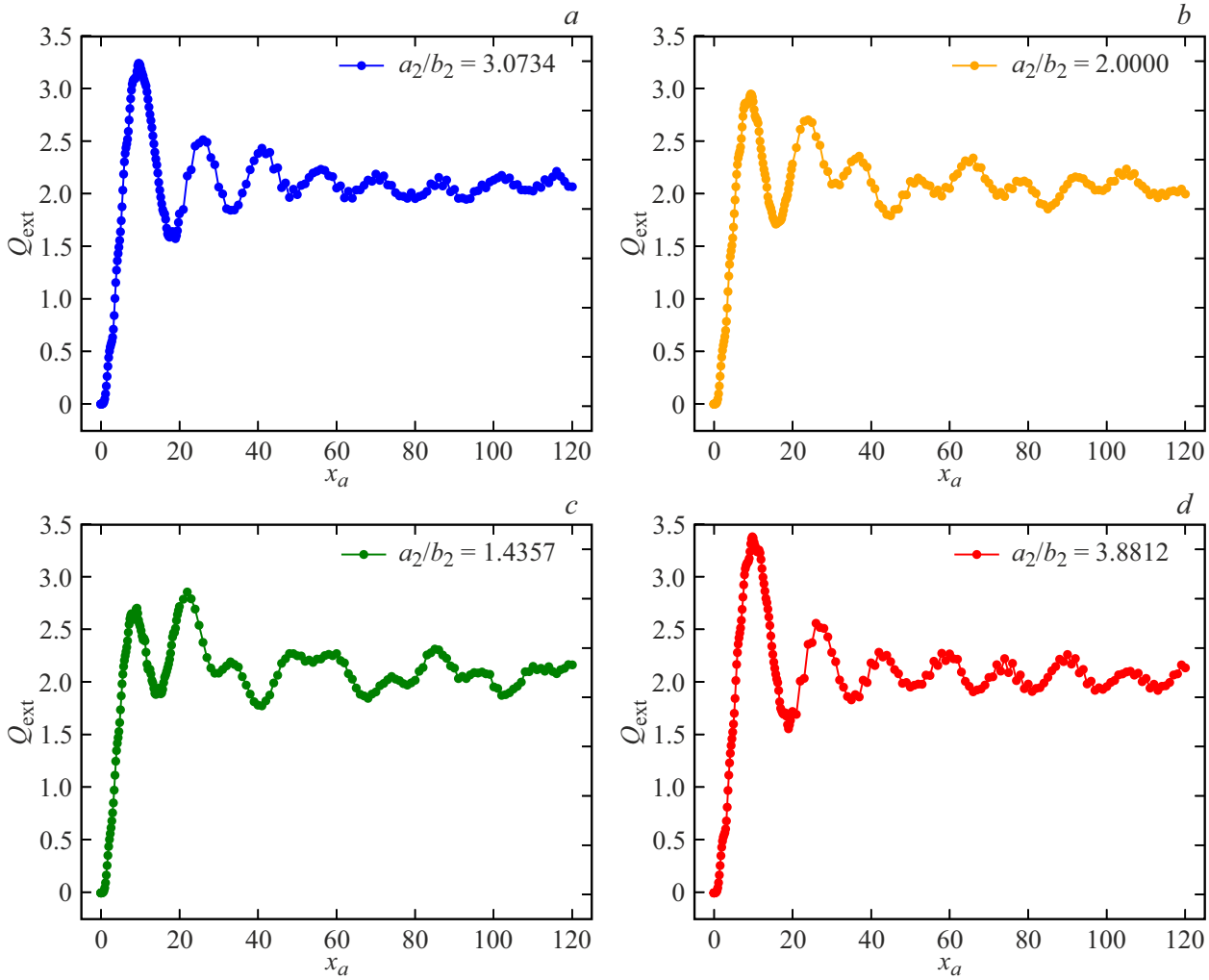

Figure 5. The same as in Figure 4, but for the two-layer flattened spheroidal particles (Table 2).

i.e. in our case $T \approx 2\pi$. The curves in Figure 4 show that, excluding the particles with the sphere-shaped core (Figure 4, *c*), 8.5 and 11.5 periods fall on segments [20,80] and [40,120], respectively. Thus, the theoretical evaluation in the first approximation gives $T \approx 6.3$, and the direct numerical calculation gives only 10% more: $T \approx 7.0$, which may be considered as a satisfactory agreement. Note that, for the elongated spheroids at $\alpha = 0$, equation (67) predicts an approx. 1.25 times longer period for the particles with the sphere-shaped core than for those with a very elongated core, which is generally observed in Figure 4.

For the flattened particles, the semi-major axes shall be replaced with semi-minor axes in this case, i.e. $l_1 = x_{b_1}$, $l_2 = x_{b_2}$. Since the curve in Figure 5 is plotted depending on the dimensionless linear diffraction parameter x_{a_1}, then the oscillation period increases by $a_1/b_1 = 2$ times. Direct counting on the same segments shows that the number of periods for the flattened particles (Figure 5) is twice as small as for the elongated particles.

In the perpendicular incidence ($\alpha = 90$), the oscillation behavior is inverted because now or the elongated particles $l_1 = x_{b_1}$, $l_2 = x_{b_2}$, and for the flattened particles $l_1 = x_{a_1}$, $l_2 = x_{a_2}$. As a result, the number of extreme values for the flattened particles is twice as large as for the elongated ones, and the number of peaks and valleys remains the same, i.e. 14 of both on segment [0, 100] (Figure 4 and 6). Moreover, even the extreme positions on the x axis vary insignificantly. If the incident plane wave propagates at an angle to the particle center line, then the Te- and TM-type waves are considered depending on the orientation of the electric field strength vector . In Figure 6, the corresponding lines almost merge with each other having the highest differences on segment [0, 10]. This result is supported by more detailed calculations for small particles [16]. This paper also provides a convenient model for a two-layer spheroid in the form of a homogeneous spheroidal particle with the effective refractive index $m_{ef} = [m_1(V_1 - V_2) + m_2V_2]/V_1$ that is doing well at the first stage, i.e. until the first peak.

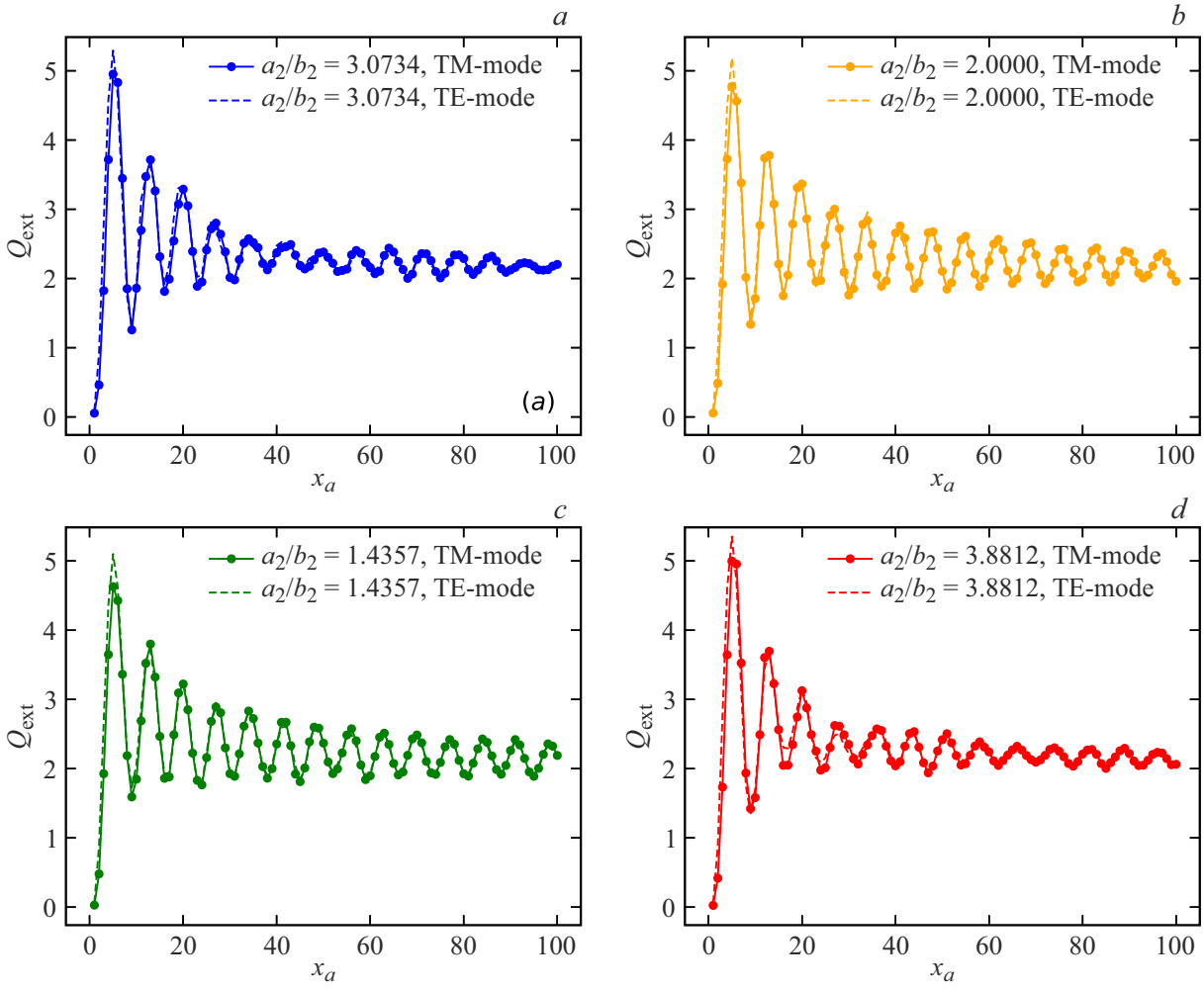

Figure 6. The same as in Figure 4, but with perpendicular incidence ($\alpha = 90°$) for the TM- and TE-modes.

The issue of geometric-optical limit of the attenuation efficiency factor for two-layer spheroidal particles is of interest. The given figures show that in accordance with the theory $Q_{ext} \to 2$ at $x_{a_1} \to \infty$ for dielectric particles and also for particles with an absorbing core (Figure 7). Whereas in the latter case this conclusion is clear, for dielectric particles the presence of a priori known geometric-optical limit is masked by oscillations that achieve their highest value for the elongated particles in the parallel radiation incidence. In general, convergence on the valleys to the limit is quite clearly pronounced, and for the peaks this trend is well traced considering the above-mentioned remark.

For two-layer spheroids with the absorbing core, behavior of the attenuation efficiency factor on the first third of the given particle size variation interval is the same as for the equivalent dielectric particles. The main difference is in the fact that the factor oscillations attenuate fast enough, i.e. they are almost absent at $x_{a_1} \geq 50$ (Figure 4). Here, a conclusion may be made that the influence of core shape on the attenuation, scattering and absorption efficiency factors is quite weak.

2.4. Influence of the core shape on the particle scattering matrix

In some provisions of the light scattering theory, besides the integral optical characteristics of scatterers (various cross-sections ,etc.), differential characteristics (scattering matrix , etc.) appear to be important. We have considered the scattering matrix component variations for two-layer spheroids with core shape variation. Some results of such calculations Some results of such calculations are given in Figure 8 that shows the components of the 4×4 scattering matrix F_{11}, F_{21} (determined according to [1]) depending on the angle θ (the scattering angle is equal to $\theta - \alpha$) in the planes $\phi = 0$ or 90° for the elongated spheroids with $x_{V_1} = 3$, the particle surface semi-axes ratio $a_1/b_1 = 2$ and shell-to-core volume ratio $(V_1 - V_2)/V_2 = 2$ in the oblique radiation incidence to the particle center line ($\alpha = 45°$). The refractive indices of the core ($m_2 = 1.5 + 0.01i$) and the shell ($m_1 = 1.3$) are typical for contaminated silicates and water ice in the visible spectrum.

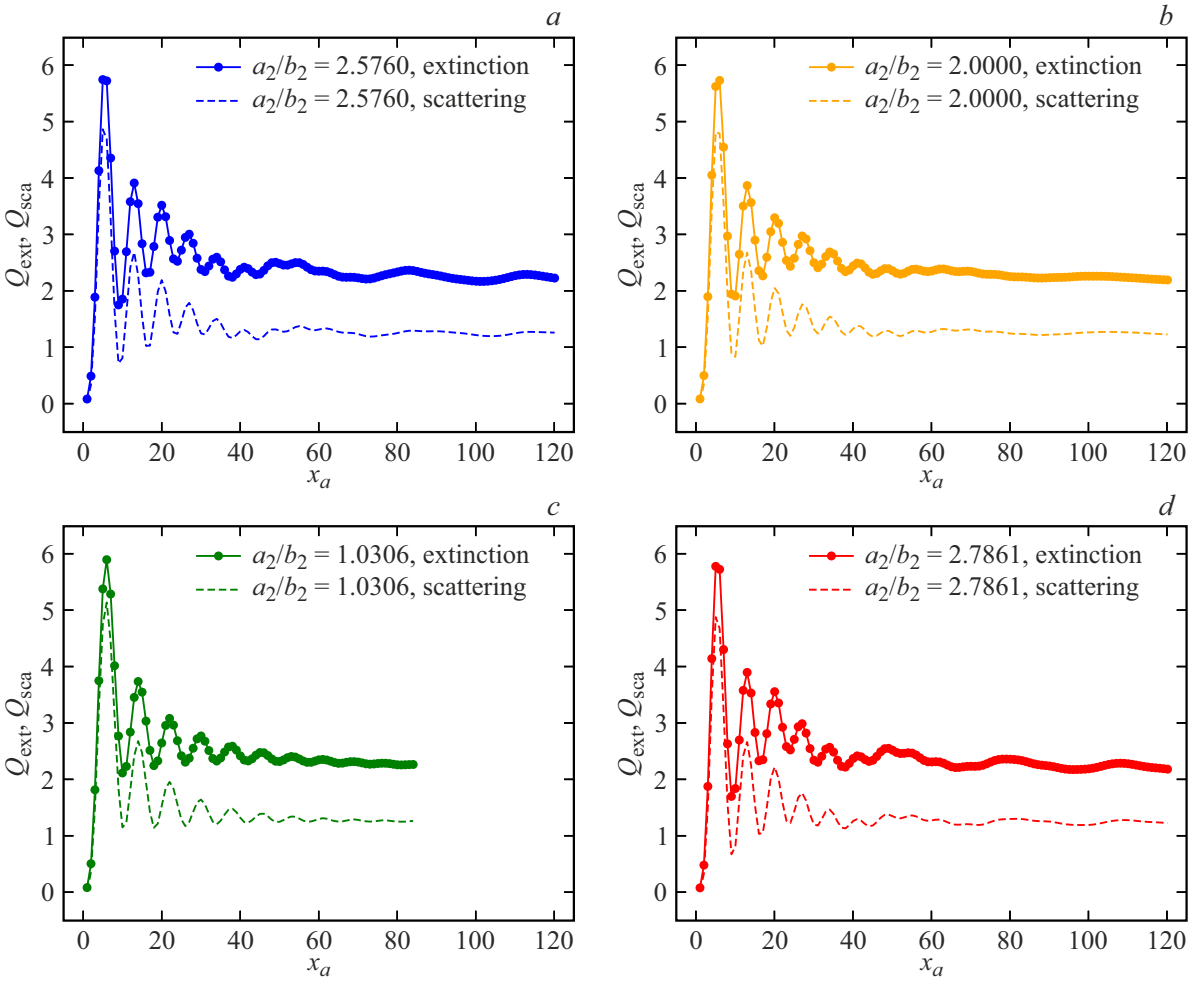

Figure 7. The same as in Figure 4, but for the attenuation and scattering efficiency factors Q_{ext} and Q_{sca} , respectively, in case of an absorbing core with the refractive index $m_2 = 1.5 + 0.05i$.

Figure 8 shows that for spheroids whose size is comparable with the wavelength ($r_V \sim \lambda$), the core shape almost does nor affect the indicatrix (F_{11}), but changes greatly the orientation and degree (F_{21}/F_{11}) of polarization of radiation scattered at large angles (the plane with ϕ equal to 0 includes the particle center line and wave vector). The particles with confocal and similar core and shell have quite similar indicatrix (and polarization).

We have also considered two-layer spheroidal particles whose core shape and relative volume did not changed, but the shell shape varied. Some results are shown in Figure 9 that gives the data for the two-layer elongated spheroids with the same core and shell volumes for the plane $\phi = 90^\circ$ (the rest parameters are as shown above). Apparently, the differences in polarization (F_{21}/F_{11}) observed in the figure for particles with different shell shape are not significant because they will be smoothed by the particle distribution by orientations and seizes that is expected in practice. On the other hand, the shell shape changes considerably the fraction of radiation scattered at large angles.

Thus, non-confocality of the core and shell of the two-layer spheroids may induce significant effects in optical properties of such scatterers. Such effects are fundamentally ignored when using a confocal spheroid model widely used, for example, in astronomy.

3. Conclusion

The problem of light scattering by the spheroidal particle with non-confocal layer boundaries has been effectively solved for the first time using the field expansion in spheroidal bases. A solution algorithm provided includes the main recent theoretical achievements: employment of a new spheroidal function normalization, exclusion of the complex TE-mode from consideration, transition from the spheroidal T-matrix to a regular spherical one, etc.

Using the procedures for spheroidal function calculation that had been recently created by van Buren, a program was written to implement the proposed algorithm in case of two-layer spheroids. Convergence and accuracy of the

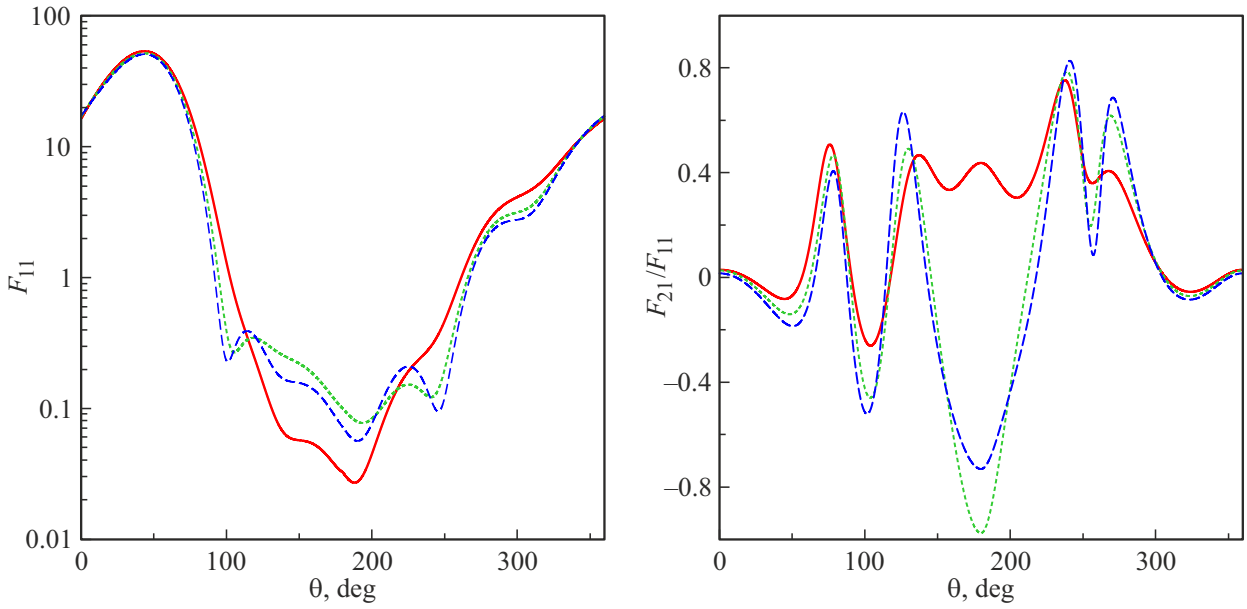

Figure 8. The scattering matrix componentF_{11} and F_{21}/F_{11} depending on the scattering angle θ in the planes $\phi = 0$ or 90° for the elongated two-layer spheroids with different core shapes: $a_2/b_2 = 1.001$ (red solid lines), 2 (green dotted lines), 2.82 (blue dashed lines). Oblique radiation incidence ($\alpha = 45^\circ$), particle diffraction parameter $x_{V_1} = 3$, shell-to core volume ratio ($a_1/b_1 = 2$) is equal to 2:1 with the refractive indices $m_1 = 1.3$ and $m_2 = 1.5 + 0.01i$, respectively.

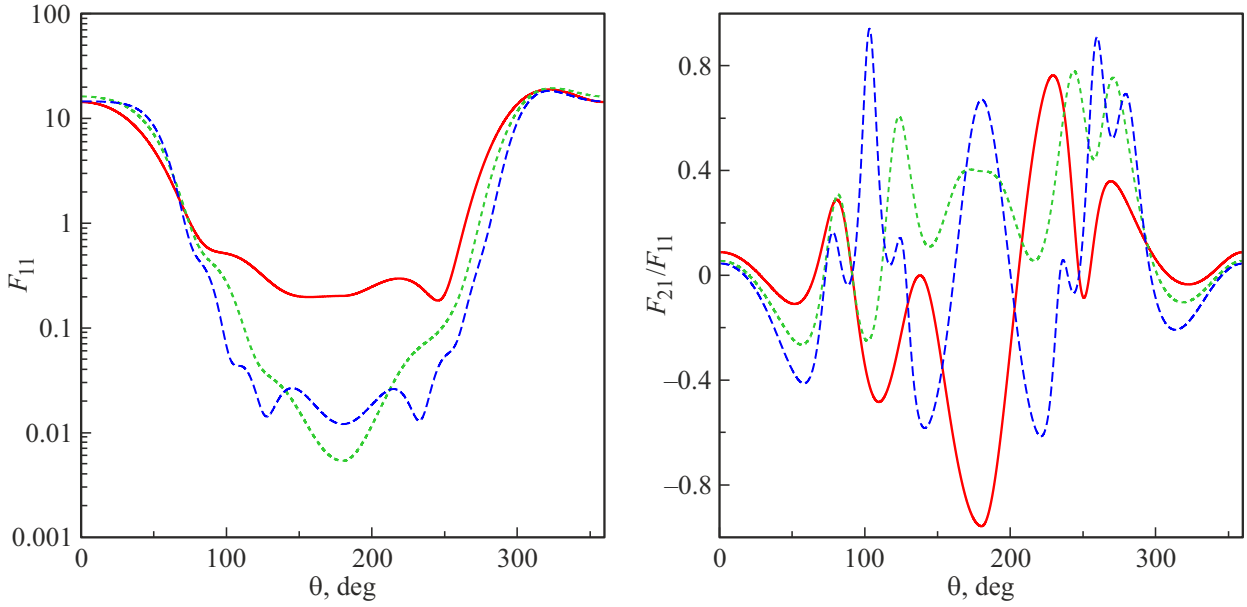

Figure 9. The same as in Figure 8, but in plane $\phi = 0$ for elongated two-layer spheroids with different shell shapes: $a_1/b_1 = 4.45$ (red solid lines), 2.5 (green dotted lines), 4 (blue dashed lines). Oblique radiation incidence ($\alpha = 45^\circ$), plane $\phi = 90^\circ$, particle diffraction parameter $x_{V_1} = 3$, equal shell and core volumes ($a_2/b_2 = 2$), whose refractive indices are equal to $m_1 = 1.3$ and $m_2 = 1.5 + 0.01i$, respectively.

solution have been investigated for spheroidal particels with four types of codes: confocal to the shell, similar to the shell, most sphere-shaped and most elongated/flattened with the specified particle shape and core-to-shell volume ratio.

Cross-section calculation data for the two-layer spheroids of the specified types with high diffraction parameter values (up to $x_a = 2\pi a/\lambda = 120$) has been reviewed. Similar numerical results for layered spheroids has been compared with approximate abnormal diffraction theory. Calculations of the scattering matrix components are also provided to show that the usually addressed layered spheroids with confocal layer boundaries describe well the optical

properties of only those particles whose core and shell are similar in shape. It is noted that new optical effects may be also observed for two-layer spheroids of another type, i.e. for particles with the same core shape, but different shell (particle) shape.

Acknowledgments

The authors are grateful to A.L. van Buren for the created spheroidal function calculation programs that are freely available on the Internet.

Funding

The efforts of V.F. on theoretical study of light scattering by layered spheroids was supported by the Ministry of Science and Higher Education of the Russian Federation, grant FSRF-2023-0003, efforts of V.I. and D.T. on creation of software for simulation of light scattering by layered spheroids and calculation of their optical properties – by grant 20-72-10052 of the Russian Science Foundation.

Conflict of interest

The authors declare that they have no conflict of interest.

References

[1] K. Bohren, D. Huffman, *Pogloscheniye i rasseyaniye sveta malymi chastitsami* (Mir, M., 1986) (in Russian).
[2] M.I. Mishchenko, J.W. Hovenier, L.D. Travis. *Light scattering by nonspherical particles* (Academic Press, San Diego, 2000). DOI: 10.1088/0957-0233/11/12/705
[3] M.I. Mishchenko, L.D. Travis, A.A. Lacis. *Scattering, absorption and emission of light by small particles* (Cambridge Univ. Press, Cambridge, 2002).
[4] V.V. Klimov. *Nanoplazmonika* (Fizmatlit, M., 2010) 480 s. (in Russian).
[5] H.C. van de Hulst. *Light scattering by small particles* (Dover Publ., New York, 1957).
[6] A.A. Kokhanovsky. *Light scattering media optics: problems and solutions* (Wiley-Praxis, Chichester, 1999).
[7] F.M. Kahnert. JQSRT, **79**–**80**, 775 (2003). DOI: 10.1016/S0022-4073(02)00321-7
[8] V.G. Farafonov, V.B. Il'in, M.S. Prokopjeva. JQSRT, **79**–**80**, 599 (2003). DOI: 10.1016/S0022-4073(02)00310-2
[9] V.G. Farafonov, V.B. Il'in. *Light Scattering Reviews* (Springer-Praxis, Berlin, 2006), p. 125. DOI: 10.1007/3-540-37672-0_4
[10] A.A. Vinokurov, V.G. Farafonov, V.B. Il'in. JQSRT, **110**, 1356 (2009). DOI: 10.1016/j.jqsrt.2009.02.031
[11] V.G.Farafonov, V.I. Ustimov, M.V.Sokolovskaya. Opt. Spectrosc., **120**, 448 (2016). DOI: 10.1134/S0030400X16030073
[12] V.G.Farafonov. Opt. Spectrosc., **117**, 923 (2014). DOI: 10.1134/S0030400X1412008X
[13] V.G.Farafonov, V.B. Il'in. Opt. Spectrosc., **115**, 745 (2013). DOI: 10.1134/S0030400X13110052
[14] V.G.Farafonov, A.A. Vinokurov. Opt. Spectrosc., **105**, 118 (2008). DOI: 10.1134/S0030400X08080201
[15] T. Onaka. Ann. Tokyo Astron. Observ., **18**, 1 (1980).
[16] V. Farafonov, N. Voshchinnikov, V. Somsikov. Appl. Opt., **35**, 5412 (1996). DOI: 10.1364/AO.35.005412
[17] I. Gurwich, M. Kleiman, N. Shiloah, B. Oaknin. JQSRT, **79**–**80**, 649 (2003). DOI: 10.1016/S0022-4073(02)00312-6
[18] V.G. Farafonov, N.V. Voshchinnikov. Appl. Opt., **51**, 1586 (2012). DOI: 10.1364/AO.51.001586
[19] V.G. Farafonov. J. Math. Sci., **175**, 698 (2011). DOI: 10.1007/s10958-011-0384-9
[20] Y. Han, H. Zhang, X. Sun. Appl. Phys., **B 84**, 485 (2006). DOI: 10.1007/s00340-006-2298-7
[21] V.G.Farafonov. Opt. Spectrosc., **114**, 421 (2013). DOI: 10.1134/S0030400X13030090
[22] V.G.Farafonov, V.B. Il'in, D.G.Turichina. Opt. Spectrosc., **130**, 251 (2022). DOI: 10.21883/EOS.2022.02.53686.2893-21
[23] M. Kerker. *The scattering of light and other electromagnetic radiation* (Academic Press, New York, 1969). DOI: 10.1016/C2013-0-06195-6
[24] N.V. Voshchinnikov, V.G. Farafonov. Astrophys. & Space Sci., **204**, 19 (1993). DOI: 10.1007/BF00658095
[25] V.B. Il'in, D.G. Turichina, V.G. Farafonov et al. JQSRT, **311**, 108759 (2023). DOI: 10.1016/j.jqsrt.2023.108759
[26] V.I. Komarov, L.I. Ponomarev, S.Yu. Slavyanov. *Sferoidalnye i kulonovskiye sferoidalnye funktsii* (Nauka, M., 1976) (in Russian).
[27] C. Flammer. *Spheroidal wave functions* (Stanford Univ. Press, Stanford, 1957).
[28] J. Meixner, F.W. Schäfke. *Mathieusche Funktionen and Sphäroidfunktionen* (Springer, Berlin, 1954).
[29] A.L. van Buren. arXiv-preprints, math/2009.01618 (2020). DOI: 10.48550/arXiv.2009.01618
[30] J. Ding, P. Yang. Opt. Express, **31**, 40937 (2023). DOI: 10.1364/OE.505416
[31] V.G.Farafonov, V.B. Il'in, D.G.Turichina. Opt. Spectrosc., **131**, 649 (2023). DOI: 10.1134/S0030400X23060048
[32] V.G. Farafonov, N.V. Voshchinnikov, E.G. Semenova. J. Math. Sci., **214**, 382 (2016). DOI: 10.1007/s10958-016-2784-3
[33] P.W. Barber, S.C. Hill. *Light scattering by particles: computational methods* (World Scientific, Singapore, 1990). DOI: 10.1142/0784

Translated by EgoTranslating